Int. J. Multiphase Flow Vol. 19, No. 5, pp. 765–795, 1993
Printed in Great Britain.

0301-9322/93 $6.00 + 0.00

TEMPERATURE AND VELOCITY FIELDS IN TURBULENT LIQUID FLOW ADJACENT TO A BUBBLY BOILING LAYER

R. P. ROY, A. HASAN† and S. P. KALRA‡
Department of Mechanical and Aerospace Engineering, Arizona State University, Tempe, AZ 85287-6106, U.S.A.

(Received 17 October 1991; in revised form 10 February 1993)

Abstract—Turbulent velocity and temperature fields were measured in the all-liquid region adjacent to a subcooled flow boiling layer formed at the heated inner wall of a vertical concentric annular channel. Refrigerant-113 was the working fluid and measurements were performed at two pressures and inlet liquid Reynolds numbers of 24,400 and 33,400 over a wall heat flux range of 30,000–80,000 W/m^2. Selected measurements in nonboiling turbulent liquid flow through the same channel are also presented for comparison. The data show that significant changes in the turbulent structure of the all-liquid region are brought about by its proximity to the bubbly boiling layer.

Key Words: temperature field, velocity field, bubbly layer, boiling

1. INTRODUCTION

Development of a physically realistic multidimensional two-fluid model of turbulent subcooled boiling flow depends upon the availability of quantitative information on the turbulence characteristics of the flow—for example, distribution of Reynold stress components and turbulent heat flux in the liquid (continuous) phase, shear stress and heat transfer rate at the vapor–liquid interface etc. Such information can only be obtained from fundamental experiments.

If the degree of subcooling is sufficiently high, two regions may be distinguishable in subcooled boiling flow through an annular channel whose inner wall is heated and whose outer wall is unheated (figure 1)—a region of boiling fluid adjacent to the inner wall and an all-liquid region extending from the boiling layer edge to the outer wall. The boiling layer is usually bubbly in structure and the movement of vapor bubbles through the liquid continuum can be expected to contribute additional perturbations to liquid velocity, temperature and pressure in both regions. The turbulence characteristics of the liquid phase are therefore altered. On the other hand, the liquid-phase turbulence plays an important role in the spatial distribution of the vapor bubbles and thus in the development of the flow regime downstream.

Some related experiments and model development have been carried out during the last two decades. Only those of significance to the work reported here will be reviewed briefly. Serizawa *et al.* (1975a–c) combined experiments and modeling to study the turbulence structure of bubbly air–water flows. A two-sensor electrical resistivity probe was used to measure the bubble velocity distribution, local gas fraction and the bubble impaction rate. The water velocity distribution was measured at isothermal conditions by constant temperature anemometry. Radial and axial temperature distributions due to a heated line source placed in the flow were measured by thermocouples. Transport parameters such as shear stress and eddy diffusivity of thermal energy were reported and the bubble transport mechanism was discussed. The same instrumentation was used by Michiyoshi (1978) to investigate heat transfer in air–water flow through a vertical annular channel. It was suggested that the agitation effect of gas bubbles significantly enhances the turbulent thermal diffusivity.

Herringe & Davis (1976), in their experimental study of the structure of air–water mixture flow in a vertical pipe, suggested that turbulent energy is produced in such flows by shear stresses in

†Present address: Intel Corporation, Phoenix, AZ, U.S.A.
‡Permanent address: Nuclear Power Division, Electric Power Research Institute, Palo Alto, CA 94303, U.S.A.

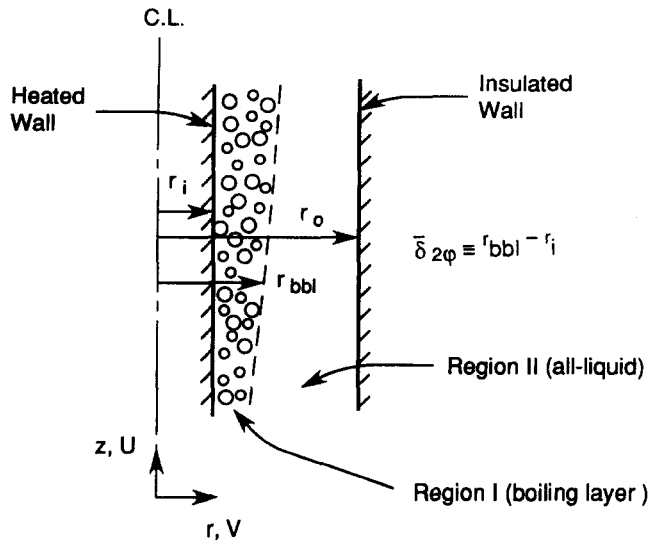

Figure 1. The boiling layer and adjacent all-liquid region in subcooled boiling flow.

the continuous phase just as it is in single-phase turbulent pipe flow. It was proposed that the turbulent energy in such mixture flows is contained both as turbulent kinetic energy and energy of the gas–liquid interfaces. A method of estimating the mean bubble size in moderate gas fraction bubbly flow based on the postulate that the turbulent energy per unit volume at any location is equally partitioned between the interfacial energy and turbulent kinetic energy was also proposed.

A theoretical and experimental study of momentum and heat transfer in turbulent bubbly gas–liquid flow was carried out by Sato *et al.* (1981a,b). It was postulated that the local, instantaneous fluctuations of velocity and temperature of the liquid are due to the superposition of two independent mechanisms, the inherent wall turbulence and the turbulence due to bubble wakes (bubble agitation). A combination of the Van Driest and Reichardt expressions for eddy momentum diffusivity was adopted for the wall turbulence contribution and a semi-empirical algebraic expression combining the local gas fraction, bubble diameter and bubble relative velocity was proposed for the bubble-generated eddy momentum diffusivity. As for the turbulent thermal diffusivity, a constant turbulent Prandtl number of unity was used for both the wall turbulence part and the part due to bubble agitation. Air–water bubbly flow experiments were performed in a vertical pipe. Local gas fraction and liquid axial velocity distributions were measured by means of an electrical resistivity probe and an impact pressure probe, respectively. Heat transfer and temperature field measurements were not performed and the theoretical predictions were compared with such measurements by others. Generally, the agreement of the predictions with the temperature distribution data was not as good as that for the velocity distributions.

Theofanous & Sullivan (1982), in their laser-Doppler velocimeter study of nitrogen–water turbulent bubbly flow in a pipe, noted that the liquid-phase turbulence controls dispersion of the gas bubbles, thus being responsible for flow regime development. At the same time, the distribution of the bubbles significantly affects the turbulence structure in the liquid. They suggested that the increase in liquid turbulence intensity was due to the relative velocity of the bubbles with respect to the liquid and the associated shear stress. A theoretical basis for the prediction of turbulence intensity in dispersed two-phase flow was proposed. Comparison of the predictions with measurements indicated good agreement.

Marié (1983) employed laser-Doppler velocimetry to measure the normal components of the Reynolds stress tensor in the liquid continuum of cocurrent air–water bubbly flow through a vertical square channel, 450 × 450 mm, at atmospheric pressure and ambient temperature. All measurements were conducted in the uniform mean flow region. Shear stress measurements were not performed. The data indicate significant increases in the normal Reynolds stresses in the presence of air bubbles. In a later paper, Marié (1987) derived the laws of friction and heat transfer for fully developed turbulent two-component upward bubbly flow in a vertical pipe. Available

experimental data on the liquid-phase mean axial velocity distribution, gas fraction distribution and temperature distribution were used to develop the models. Similarity was noted between the action of the bubbles which results in an increase in turbulence and that of a grid with a random mesh. Use of Reynolds analogy was made. Comparison with experimental data of others exhibited reasonably good agreement up to gas fractions of the order of 0.3.

Michiyoshi & Serizawa (1986) used dual-sensor hot-film anemometry to study turbulent air–water bubbly flow. Estimates of the integral length scale and the Taylor microscale were reported as were the energy spectra of Reynolds normal and shear stresses. A trend of an increase in the high frequency content of the turbulence energy spectrum due to the presence of the air bubbles was observed. A probable mechanism of "fragmentation" of the large-scale turbulence structures (eddies) into smaller-scale structures due to interaction between the bubbles and these structures was discussed.

Wang *et al.* (1987) utilized single- and multi-sensor hot-film anemometry to measure the gas-phase distribution and the liquid-phase turbulence structure in bubbly air–water up- and down-flow in a pipe. The normal and shear Reynolds stresses were measured. The local isotropy of turbulence was found to be affected by the air bubbles. The Reynolds shear stress was found to be always positive in spite of the change in sign of the mean axial velocity gradient.

Serizawa & Kataoka (1990) presented a theory for suppression of turbulence in bubbly gas–liquid flows. The rate of turbulent energy production in the liquid phase was shown to depend on the local phase fractions, the liquid mean velocity gradient and the turbulent shear stress distribution. On the other hand, the dissipation rate depends on the gradients of the turbulent velocity fluctuations and the viscous shear stress. It was shown that fluctuations induced by the relative motion between the gas bubbles and the liquid result in an enhancement of liquid-phase turbulence, whereas an increase in the gas–liquid interfacial area results in a decrease of turbulent energy (Herringe & Davis 1976). The exchange between turbulent kinetic energy and interfacial energy was postulated to be one of the important mechanisms, among possibly several others, for the reduction of turbulence which is observed in the core flow region.

Lopez de Bertodano *et al.* (1990) analyzed turbulent bubbly air–water flow in a pipe with a three-dimensional two-fluid model. A τ–ϵ model of turbulence was used for the liquid phase. A lateral lift force on the bubbles arising from the relative velocity between the phases and the liquid lateral velocity gradient was incorporated in the momentum equations. The Reynolds stress equations for the liquid phase were the same as those of Launder *et al.* (1975), except for an additional source term (a second-order tensor) from the turbulence produced due to the work that the bubbles do as they move through the liquid. Due to the lack of experimental evidence to the contrary, this source term tensor was postulated to only have diagonal elements (i.e. normal components) that are nonzero. In other words, it was postulated that all of the bubble-induced turbulent energy is partitioned among the normal components. The phase distributions predicted by the analysis compared well with experimental data for air–water up- and down-flow in vertical pipes.

Lance & Bataille (1991) used the same experimental apparatus as Marié (1983) to study the characteristics of turbulence in the liquid phase of uniform vertical bubbly air–water flow. Constant temperature anemometry in conjunction with a conical hot-film probe was used to measure some characteristics of the liquid-phase turbulence, e.g. the velocity fluctuation intensities. Laser-Doppler velocimetry was utilized to measure the off-diagonal components of the Reynolds stress tensor, e.g. the turbulent shear stress. In the limited range of experimental conditions (maximum gas fraction $\approx 3\%$, gas bubble size ≈ 5 mm, approximately homogeneous and isotropic measurement region), the turbulent shear stress was found to be small ($\lesssim 10\%$) compared to the normal stresses. The isotropy of the single-phase flow field was found to be unaltered by the introduction of bubbles. The turbulent kinetic energy of the liquid phase in bubbly gas–liquid flow increased significantly in comparison to the corresponding all-liquid flow and the energy was distributed over a wider range of wavenumbers. It was concluded that the Taylor and Kolmogorov microscales were accordingly smaller than the corresponding single-phase flow length scales. It was also proposed that the liquid-phase turbulent kinetic energy in bubbly gas–liquid flow is comprised of the inherent turbulence and velocity fluctuations caused by the motion of the bubbles (*pseudo-turbulence*).

Additional scrutiny of the literature reveals that essentially all experimental studies and theoretical analyses of the turbulent structure of gas–liquid flows have so far been restricted to isothermal air(or nitrogen)–water systems. The information obtained from these studies, while important, is not sufficient for understanding the turbulent structure of boiling flows. As the first step in our effort in this regard, we have performed measurements of the turbulent velocity and temperature fields in the all-liquid region (region II, figure 1) adjacent to the boiling layer (region I) of subcooled boiling flow in an annular channel with the inner wall heated and the outer wall insulated. The quantities measured include the radial distributions of the mean axial and radial velocity components, Reynolds stress components including shear stress, mean liquid temperature, temperature fluctuation intensity and the turbulent radial heat flux.

2. EXPERIMENTS

The Rig and Test Section

The experimental rig which has been described in detail elsewhere (Jain & Roy 1983; Hasan 1991), uses Refrigerant-113 (R-113) as the working fluid. The annular test section was comprised of an outer Pyrex pipe and a 304 stainless-steel pipe assembly of 38.6 mm i.d. and an inner seamless 304 stainless-steel tube of 15.9 mm o.d. and 1.25 mm wall. Figure 2 shows, schematically, the part of the test section where the measurements were performed. The initial 0.91 m of the 3.66 m long test section served as an unheated hydrodynamic entrance length. Heat could be supplied to the remaining 2.75 m length by resistively heating (by d.c., maximum input power = 60 kW) the inner stainless-steel tube. The velocity and temperature measurement plane was approx. 85 hydraulic diameters downstream of the beginning of the heated length. Concentricity of the annulus was maintained by means of four support vane assemblies, each assembly consisting of four 9 mm long and 1 mm thick stainless-steel vanes arranged in an X configuration, welded to the inner tube at equal axial spacings. The nearest vane assembly upstream of the measurement plane was about 31 hydraulic diameters away. Concentricity at the measurement section was further ensured by means of a flange equipped with four micrometers installed immediately downstream of the section (not shown in figure 2). The heater tube was filled with aluminum oxide powder insulation. The outer section of the annular channel was insulated with 50 mm thick jacketed fiberglass wool.

The heat flux imposed at the inner wall of the annulus during any experiment was calculated as the ratio of the product of the measured voltage drop across the heater tube and the current through it (also measured) and the tube surface area. Heat balance calculations based on the liquid mass flow rate through the test section and the increase in the mixed-mean temperature of the liquid always accounted for the heat generated in the tube wall to within $\pm 2\%$.

All measurements were carried out at nominally steady-state conditions. The dissolved air content of the Refrigerant-113 in the rig, after extensive degassing, was measured by a Seaton–Wilson Aire–Ometer to be typically 1.18×10^{-3} mol air/mol R-113. This meant that the vapor bubbles in the boiling layer contained a small amount of air.

Instrumentation and Calibrations

Figure 2 also shows the locations of a miniature three-sensor hot-film anemometer probe (TSI 1295AK-10W) and a chromel–constantan microthermocouple (P. Beckman Co., μTC-PB-03) in the measurement section (Hasan *et al.* 1992; Beckman *et al.* 1993). Two (of a total of four) copper–constantan surface thermocouples (STC) used to measure the heated tube surface temperature are shown as well.

Sensors 1 and 2 (the x-sensors) of the anemometer probe were operated in the constant temperature anemometer (CTA) mode for velocity measurement in the all-liquid region with the sensors maintained at 71°C.† The liquid temperature at the measurement plane was in the range 35–60°C so that the "overheat ratio" of the sensors was adequate. Sensor 3 was operated in the resistance thermometer (constant current) mode for the measurement of fluid temperature in both the all-liquid region and the boiling layer. An active phase-lead compensation circuit was employed

†The sensor temperature was limited by the consideration that boiling must not occur at the sensor.

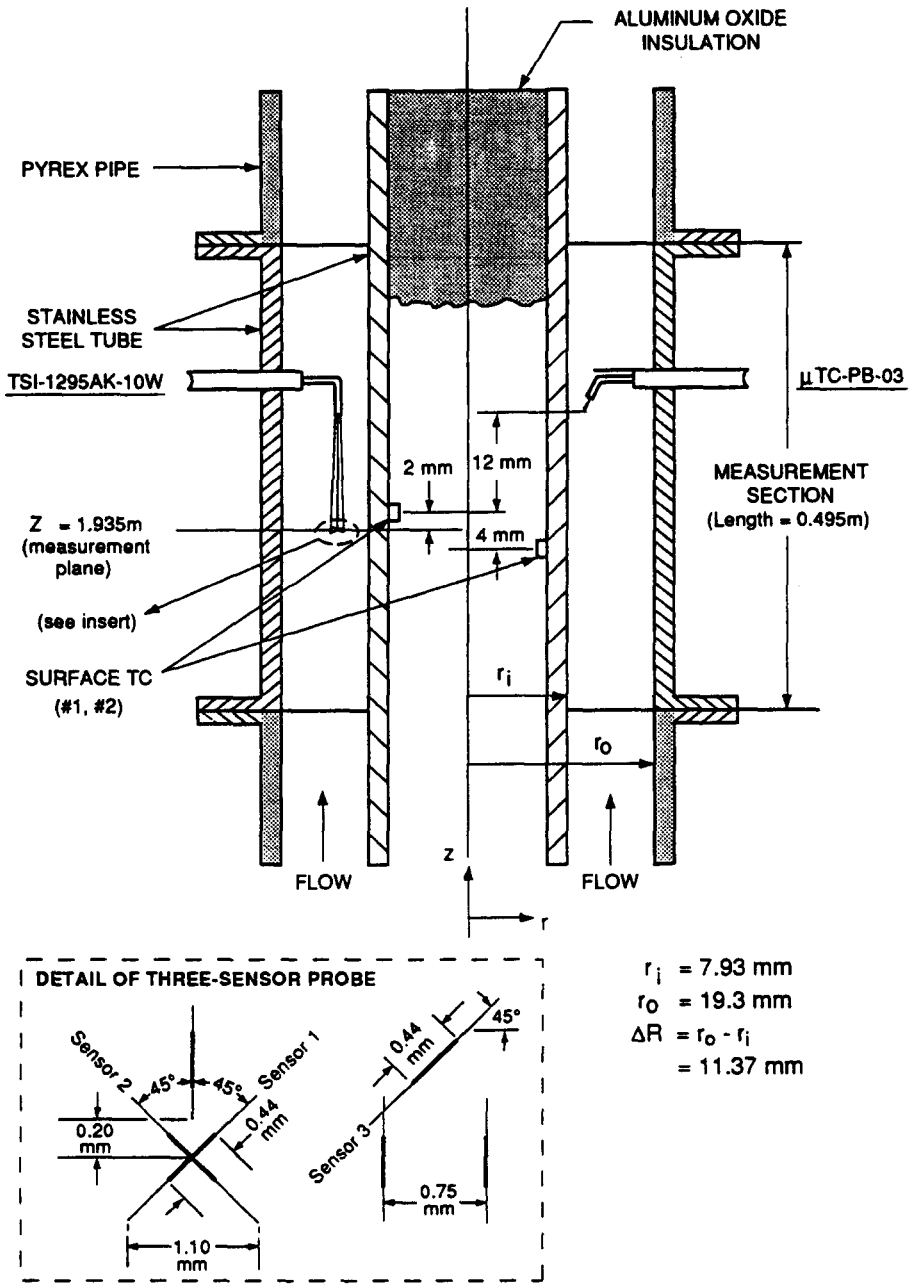

Figure 2. The annular test section.

to improve the frequency response of sensor 3 (compensated time constant ≈ 4 ms). It was hoped that the sensor would be able to distinguish the vapor-phase temperature from the liquid-phase temperature and follow the high-frequency fluctuations in liquid temperature, e.g. to 200 Hz (Hasan *et al.* 1992). It, however, was unable to respond adequately to the ambient temperature change during vapor bubble passages (the bubbles were typically $\lesssim 1$ mm) and essentially measured the *fluid* temperature (mean and fluctuation) in the boiling layer, the fluid in this region being a vapor–liquid mixture.†

The voltage output of a CTA bridge is a function of both the velocity and temperature of the ambient fluid at the sensor location. Therefore, in order that the velocity may be correctly measured

†We have, recently, been successful in this regard by switching to a specially-manufactured microthermocouple of rather small dimensions (disc junction ≈ 0.1 mm dia, 2.5 μm thick) and a smaller time constant (≈ 3.4 ms).

in a nonisothermal flow field, the output must be rendered independent of the fluid temperature. To this end, two temperature compensation circuits were built to permit on-line compensation of the CTA outputs (Hasan *et al.* 1992). Each temperature-compensated CTA output signal was linearized on-line and extensive velocity calibration of the x-sensors carried out. Invariance of the velocity calibrations with respect to the ambient liquid temperature was verified over the temperature range of our experiments.

Temperature calibration of sensor 3 was performed *in situ* by increasing the liquid temperature in the test section in stages by means of an upstream preheater and by controlling the heat removed through the rig heat exchanger. The test section itself remained unheated. The microthermocouple which had been calibrated earlier in a constant temperature bath provided the reference temperature during this calibration. The heater tube surface thermocouples were also calibrated *in situ* in this manner.

In an earlier series of experiments, a miniature single-sensor hot-film anemometer probe (TSI 1212AS-10A; 25 μm dia, 250 μm length, uncoated) had been used in a modified CTA mode (with nucleate boiling established at the sensor surface) to determine the radial extent of the boiling layer and the vapor fraction distribution at approximately the same measurement plane (Hasan *et al.* 1991). All conditions of interest for the present measurements (as given by the wall heat flux, fluid mass velocity, pressure and temperature) were covered by those experiments.

A dedicated system (DATA 6000A, Analogic) with a floppy disk drive and plotter peripherals was used to acquire, store, analyze and display the time series data for velocity and temperature.

Tests

Table 1 shows the range of variables over which the measurements were conducted and the associated uncertainties.

A steady state was established in the test section at each nominal experimental condition. The heated wall temperature at the measurement plane was measured by STC # 1 and STC # 2. The three-sensor hot-film probe was manually traversed across the all-liquid region and time series data (typically, 16.384 s record length with a sampling period of 1 ms) were acquired with each sensor at each radial location. The 1 ms sampling period was considered to be appropriate because of the relatively large spatial separation between the hot-film sensors and its consequent inability to resolve the smaller length scales of turbulence. For example, considering a 0.7 mm separation between two sensors, the time period (i.e. frequency^{-1}) associated with a 0.5 m/s flow velocity would be approx. 1.4 ms.

The following quantities were obtained from the data:

mean liquid axial velocity, $\bar{U}$
mean liquid radial velocity, $\bar{V}$
mean liquid temperature, $\bar{T}$
turbulence intensities, $(\overline{u^2})^{0.5}$, $(\overline{v^2})^{0.5}$, $(\overline{t^2})^{0.5}$
Reynolds shear stress, $\overline{uv}$
single-point cross-correlation between radial velocity and temperature fluctuations, $\overline{vt}$.

The measurements were continued across the boiling layer (region I) boundary into the layer itself, although the velocity field data became meaningless due to the limitations of our sensors.

Table 1. Range of experiments and measurement uncertainties[a]

	Range	Uncertainty
Mass velocity (kg/m^2 s)	579–801	±3
Wall heat flux (W/m^2)	0–35,000	±80
	36,000–80,000	±150
Wall temperature (°C)	70–95	±0.4
R-113 partial pressure at measurement plane (kPa)	219–253	±0.7
Mean liquid temperature at test section inlet (°C)	35–43	±0.1
Sensor radial traverse (μm)	0–10,000	±40

[a]The uncertainty estimates are for 95% confidence.

Table 2. Range of turbulence quantities and associated uncertainties[a]

	Range	Uncertainty
Mean axial velocity (m/s)	0.35–0.65	± 0.006
Axial velocity fluctuation intensity (m/s)	0.025–0.100	± 0.002
	0.100–0.175	± 0.004
Radial velocity fluctuation intensity (m/s)	0.020–0.080	± 0.002
	0.080–0.125	± 0.004
Reynolds shear stress (m^2/s^2)	(-800×10^{-6})–(2700×10^{-6})	$\pm 15 \times 10^{-6}$ for magnitude $< 100 \times 10^{-6}\ m^2/s^2$ $\pm 50 \times 10^{-6}$ for magnitude between 100×10^{-6} & 900×10^{-6} $\pm 150 \times 10^{-6}$ for magnitude between 900×10^{-6} & 2700×10^{-6}
Temperature fluctuation intensity (°C)	0.25–2.8	± 0.02
Cross-correlation between radial velocity and temperature fluctuations (m°C/s)	(2.0×10^{-3})–(27.0×10^{-3})	$\pm 0.4 \times 10^{-3}$ for magnitude $< 5.0 \times 10^{-3}$ $\pm 0.7 \times 10^{-3}$ for magnitude $> 5.0 \times 10^{-3}$

[a]The uncertainty estimates are for 95% confidence.

Specifically, neither the x-sensors operating in the CTA mode nor the temperature sensor (as discussed earlier) were able to provide reliable discrimination between the vapor and the liquid phases.

Table 2 contains the measured range of values of the turbulence quantities and the uncertainties associated with them.

3. RESULTS AND DISCUSSION

Boiling Layer Thickness

Figure 3 shows the subcooled flow boiling layer thickness, $\bar{\delta}_{2\phi}$, as a function of the wall heat flux for various combinations of two mass velocities, two measurement plane pressures and two inlet subcoolings. ΔR is the radial gap between the annulus walls, i.e. $(r_o - r_i)$. The outer edge of the boiling layer, defined here as the radial location in the fluid where the vapor residence time fraction becomes essentially zero, was determined from measured radial vapor fraction profiles. Figure 4 shows, as an example, radial vapor fraction profiles at the measurement plane for five different heat fluxes and the following fluid condition:

mass velocity = 801 kg/m^2 s
R-113 pressure at m.p. = 253 kPa
inlet temperature of liquid = 43.0°C.

The nondimensional radial position R^* in figure 4 is defined as $(r - r_i)/(r_o - r_i)$. Additional vapor fraction profiles can be found in Hasan *et al.* (1991) and Hasan (1991).

The data in figure 3 exhibit several expected trends: (i) at the same mass velocity, pressure and inlet subcooling, the boiling layer thickness at any given axial location increases monotonically with the wall heat flux (until the layer occupies the entire annulus); (ii) the layer thickens as the pressure is lowered while the other experimental parameters are maintained the same; (iii) a higher liquid-phase temperature (i.e. a lower liquid phase subcooling) results in a thicker boiling layer; and (iv) for the same wall heat flux, pressure and inlet subcooling, the boiling layer thickens when the mass velocity is decreased.

The boiling layer thickness data helped direct the turbulence measurement experiments.

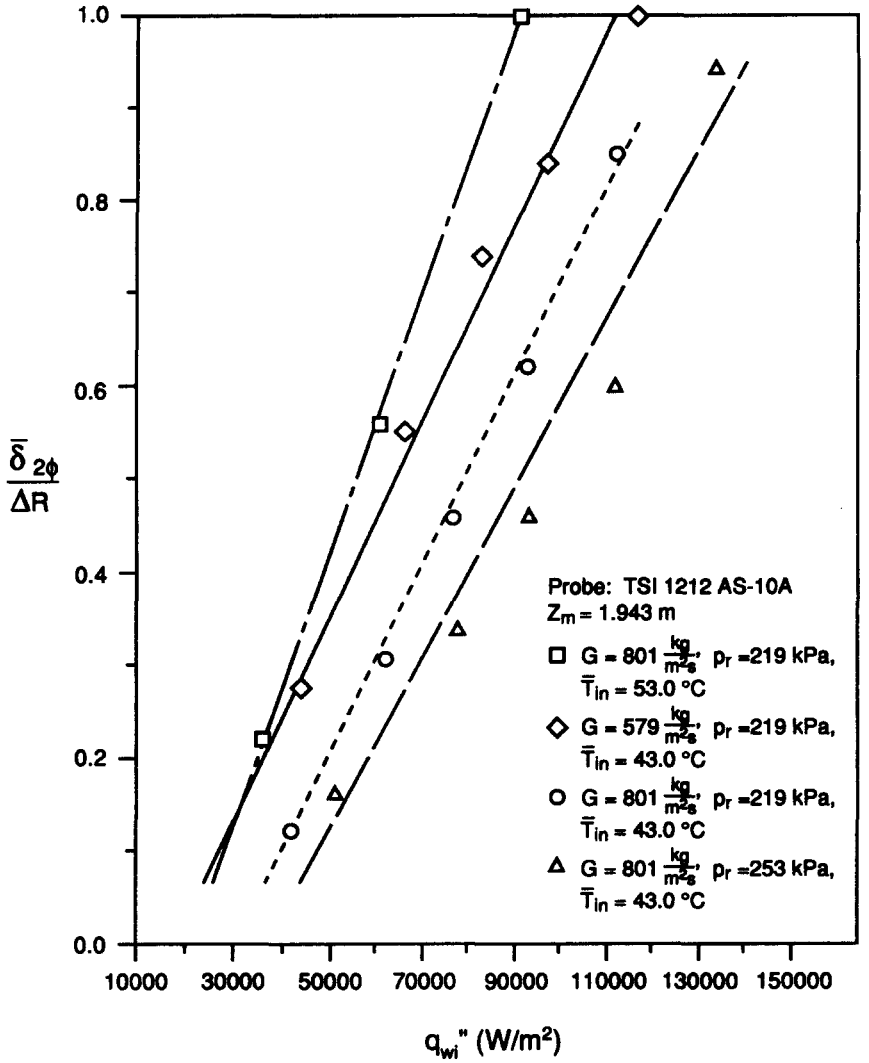

Figure 3. Variation of boiling layer thickness with wall heat flux.

Temperature Field

Mean fluid temperature

Figure 5(a) shows radial profiles of the mean fluid temperature in subcooled boiling flow at a mass velocity of 801 kg/m² s, four different wall heat fluxes, an R-113 pressure (at m.p.) of 219 kPa and an inlet liquid temperature of 43.0°C. On each profile, the location of the boiling layer outer edge is marked by a short vertical line. A mean liquid temperature profile for nonboiling flow at the same mass velocity is also shown for comparison. The measured heated wall temperature is shown in each case.

As mentioned earlier, the hot-film temperature sensor was unable to provide a clear distinction between the vapor and liquid temperatures.† Recent measurements in similar flows with a microthermocouple indicate that inside the boiling layer the mean liquid temperature is slightly lower than the mean fluid temperature (e.g. at $R^* \approx 0.1$ by 0.5–1.0°C), the actual difference depending mainly on the local vapor fraction.

†A typical method of extracting this information is to construct a probability density function (PDF) of the fluid temperature signal. Two peaks, one corresponding to vapor temperature and the other to liquid temperature, with a distribution around each, would ideally appear for subcooled boiling flow.

The data in figure 5(a) exhibit the expected trends with respect to the variation in wall heat flux. Figures 5(b) and 5(c) contain data which exhibit the influence of fluid pressure and mass velocity, respectively, on the heated wall temperature and mean fluid temperature distribution. Figure 5(b) indicates that the temperature of the heated wall is significantly affected by pressure (and, of course, heat flux). As for the fluid temperature, we, unfortunately, could not approach the wall any closer than $R^* \approx 0.13$ because of the anemometer probe stem size. In the domain $R^* \gtrsim 0.13$, which includes a portion of the boiling layer, the influence of pressure on the fluid temperature is seen to be minimal. Given the effect on the heated wall temperature, the pressure influence can be expected to increase as the wall is approached.

It appears, on the basis of the data of figure 5(c), that the fluid mass velocity affects the mean fluid temperature inside the boiling layer in essentially the same manner as it affects the temperature in the (outer) all-liquid region.

Fluid temperature fluctuation intensity

Figure 6(a) shows radial profiles of the fluid temperature fluctuation intensity for the same experimental conditions as in figure 5(a). No dramatic changes in the intensity distribution are apparent inside the boiling layer. That the intensity increases with wall heat flux in a known effect in single-phase liquid flow as is the flattening trend in the intensity as the heated inner wall is approached at moderate to high Reynolds numbers (Roy *et al.* 1986; Hasan *et al.* 1990).

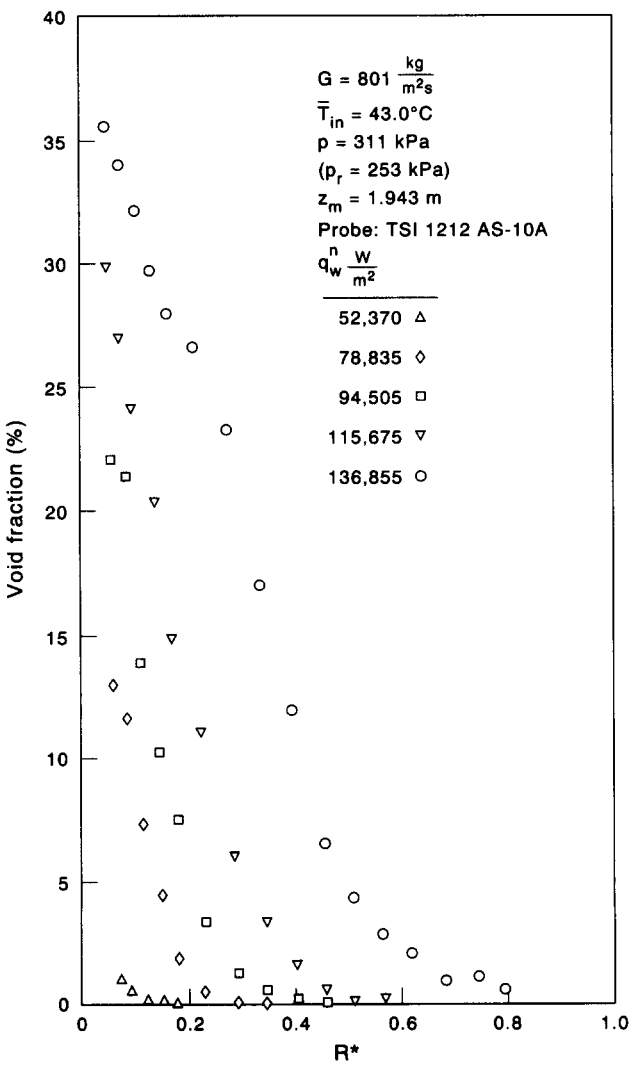

Figure 4. Vapor residence time fraction profiles in the boiling layer.

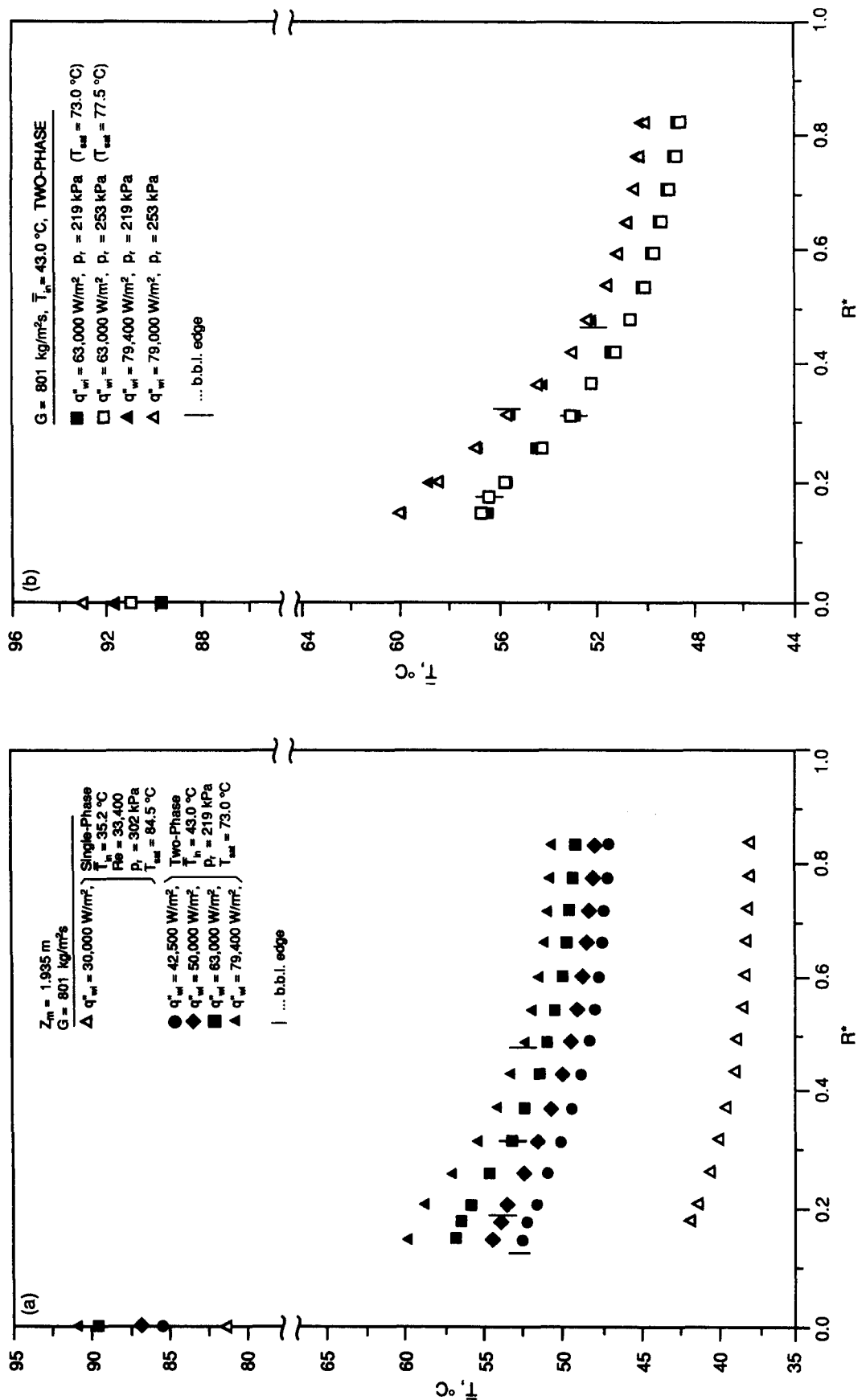

Figure 5(a, b)—*legend opposite.*

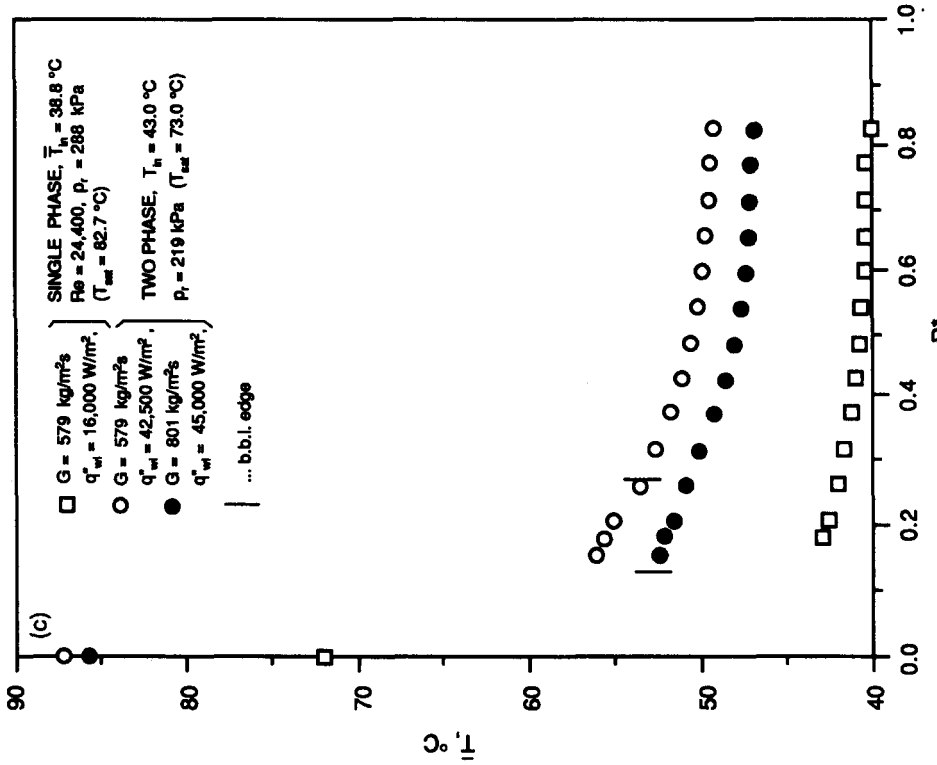

Figure 5(a–c). Mean fluid temperature profiles.

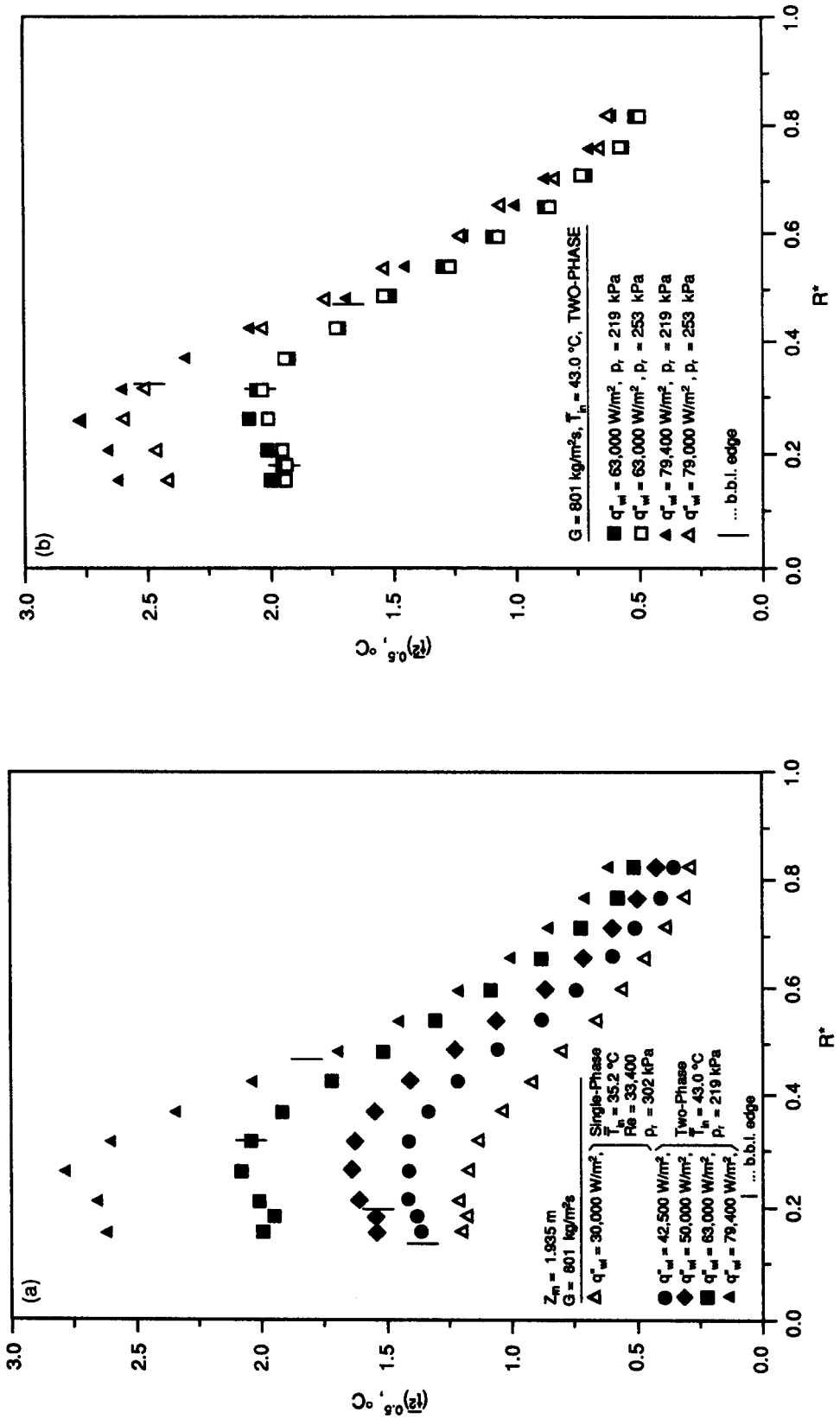

Figures 6(a, b)—*legend opposite.*

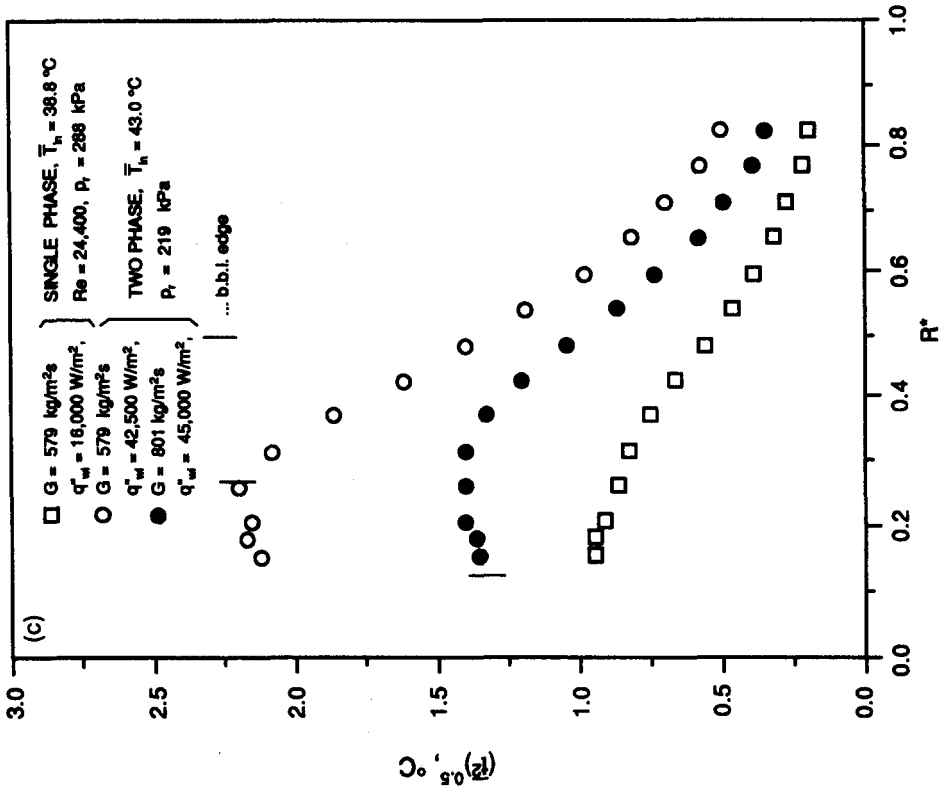

Figure 6(a–c). Fluid temperature fluctuation intensity profiles.

Figures 6(b) and 6(c) contain fluid temperature fluctuation intensity data for the same experimental conditions as in figures 5(b) and 5(c), respectively. Figure 6(b) indicates that the intensity is noticeably higher at the lower pressure (other experimental parameters remaining the same) in the boiling layer where passages of vapor bubbles and the associated high-temperature liquid layers are more frequent. The effect on the temperature fluctuation intensity in the all-liquid region is minimal however. Figure 6(c) points to a significant increase in the intensity in both the boiling layer and the all-liquid region at the lower mass velocity. It is well-known that in single-phase liquid flow at any specific wall heat flux, the temperature fluctuation intensity increases with a decrease in mass velocity (Hasan *et al.* 1990). The trend in figure 6(c) could be interpreted as the combined effect of the increase in the inherent liquid temperature fluctuation and that due to the presence of vapor bubbles.

Velocity Field

Turbulent velocity field measurements were conducted in the all-liquid region up to the boiling layer edge.

Mean axial velocity

Figure 7(a) shows radial profiles of the mean liquid axial velocity for subcooled boiling flow conditions at a mass velocity of 801 kg/m^2 s, a pressure of 219 kPa, a test section inlet temperature of 43.0°C and four different wall heat fluxes. Also shown for comparison are two velocity profiles for nonboiling flow (one being for isothermal condition) at the same mass velocity. The location of the boiling layer outer edge is marked by a short vertical line on each boiling flow profile.

The mean axial velocity profile for the two single-phase experiments exhibits the well-known feature of having a maximum at $R^* \approx 0.4$ (Brighton & Jones 1964; Hasan *et al.* 1992). Two noteworthy changes occur upon establishment of the boiling layer at the inner wall: (i) the mean liquid axial velocity increases across much of the all-liquid region (except near the outer wall), this effect becoming more pronounced at the higher wall heat fluxes; and (ii) the maximum axial velocity location shifts slightly toward the inner wall (i.e. toward the boiling layer)—e.g. from $R^* \approx 0.40$ to $R^* \approx 0.38$ at wall heat fluxes of 42,500, 50,000 and 63,000 W/m^2. Note that the boiling layer outer edges for the above three cases are at $R^* \approx 0.13$, 0.20 and 0.31, respectively. At a wall heat flux of 79,400 W/m^2, the edge of the boiling layer extends to $R^* \approx 0.48$, the all-liquid region maximum mean axial velocity being at the same location.

One reason for the observed increase in the mean axial velocity over much of the all-liquid region may be suggested: the bubbles as well as the liquid in the boiling layer flow downstream with a higher velocity than liquid in a nonboiling condition. This causes the mean axial velocity of the liquid adjacent to the boiling layer to increase (momentum transport or shear stress effect). The extent of this increase diminishes gradually as the annulus outer wall is approached. The sign and magnitude of the radial gradient of the mean liquid axial velocity (the mean strain rate), $\partial \bar{U}/\partial r$, have, in conjunction with the sign and magnitude of Reynolds shear stress, important implications for both the kinetic energy of the mean flow and the production of turbulence. Note, for instance, that at the highest heat flux (79,400 W/m^2) $\partial \bar{U}/\partial r$ is negative throughout the all-liquid region (this region occupies approximately the outer half of the annular gap for this case). At the next high heat flux (63,000 W/m^2), $\partial \bar{U}/\partial r$ is again negative in the all-liquid region except very close to the boiling layer edge where it is positive. The ramifications of these facts will be discussed when the turbulent shear stress data are presented.

Figure 7(b) depicts the influence of local pressure on the mean axial velocity distribution in the all-liquid region at two different wall heat fluxes. The other parameters, viz. mass velocity and test section inlet temperature, have been kept invariant here. At the lower of the two pressures for which data are shown, the liquid axial velocity is higher. This can again be partly attributed to the drag exerted by the higher vapor fraction boiling layer. Figure 7(c) shows the influence of mass velocity on the all-liquid region mean axial velocity distribution. Data for one single-phase liquid experiment at the lower mass velocity (579 kg/m^2 s) is also shown for comparison. The trends are clear and readily explained.

Mean radial velocity

Figure 8(a) contains radial distributions of the mean radial velocity in the all-liquid region for the same experimental conditions as in figure 7(a). The zero heat flux (isothermal) data generally exhibit the smallest magnitudes (the magnitude should ideally be zero for fully developed flow) with the data for nonisothermal single-phase liquid flow at a wall heat flux of 30,000 W/m^2 having slightly higher magnitudes. Upon commencement of boiling, the mean radial velocity of the liquid in the proximity of the boiling layer increases. An explanation is that the developing boiling layer pushes the adjacent liquid radially outward (on average). The velocity is still quite small however, being $<5\%$ of the mean liquid axial velocity in the core flow.

Figures 8(b) and 8(c) show radial profiles of the mean liquid radial velocity for the experimental conditions of figures 7(b) and 7(c), respectively. The data generally exhibit characteristics similar to those of the data in figure 8(a).

Axial velocity fluctuation intensity

Figure 9(a) shows radial distributions of the axial velocity fluctuation intensity in the all-liquid region for the same experimental conditions as in figure 7(a). Significant increases in the intensity with wall heat flux and a strong effect in the proximity of the heated wall have been reported previously by the authors for single-phase flows (Hasan *et al.* 1992). In view of the augmented energy input (as heat) to the flow, an increase in the turbulent energy production and therefore in the normal stresses is expected. A dramatic increase in the fluctuation intensity is observed when the boiling layer forms, the increase being especially marked near the edge of the layer. Augmentation in velocity fluctuations are clearly caused by the motion of bubbles in the adjoining boiling layer [pseudo-turbulence (Lance & Bataille 1991)]. A similar trend *vis a vis* temperature fluctuation intensity should be noted, figure 6(a). Scrutiny of the frequency spectrum of the axial velocity fluctuation indicates that a significant portion of the additional fluctuation energy resides at higher frequencies (e.g. 20–200 Hz), the implication being that the turbulence in the liquid adjacent to the boiling layer has a smaller microscale (e.g. Kolmogorov) compared to the corresponding single-phase liquid flow. Similar trends have been reported by other investigators (e.g. Sato *et al.* 1981a,b; Serizawa & Kataoka 1990; Lance & Bataille 1991). The increase in turbulence energy accompanied by a decrease in the smallest length scales of turbulence can be explained in terms of stretching of vortices by the mean strain rate field (Tennekes & Lumley 1972).

Figures 9(b) and 9(c) depict the axial velocity fluctuation intensity profiles for the experimental conditions of figures 7(b) and 7(c). The influence of pressure on the intensity is seen to be minimal, figure 9(b). In view of the fact that the boiling layer is thicker with a higher vapor content at the lower pressure and our earlier finding that the mean liquid axial velocity is generally higher at the lower pressure, figure 7(b), the trend in figure 9(b) seems somewhat surprising. It is interesting to note that the temperature fluctuation intensity in the all-liquid region also exhibited this lack of sensitivity to a change in pressure, figure 6(b). The intensity is, on the other hand, significantly higher, especially near the boiling layer at the lower of the two mass velocities, figure 9(c). The temperature fluctuation intensity shows a similar behavior, figure 6(c).

Radial velocity fluctuation intensity

Figure 10(a) contains radial profiles of this intensity in the all-liquid region for the experimental conditions of figure 7(a). The alteration of the radial velocity fluctuation intensity in response to changes in the adjoining boiling layer brought about by wall heat flux increases is qualitatively similar to the alteration of the axial velocity fluctuation intensity. The magnitudes of the axial and radial intensities are, however, not equal at any radial location, i.e. the turbulence is anisotropic, figure 11. It is apparent from this figure that the extent of anisotropy increases somewhat upon introduction of heat flux at the wall, even when the flow remains all-liquid. Appearance of the boiling layer does not seem to bring about any further significant changes in the anisotropy.

A noteworthy feature in figures 8(a) and 10(a) is that the relative increase in the radial velocity fluctuation intensity is markedly larger than the increase in the mean liquid radial velocity in the all-liquid region. This connotes that the radial velocity field induced in the all-liquid region by the vapor bubbles in the adjoining boiling layer is essentially random in nature with a rather small mean

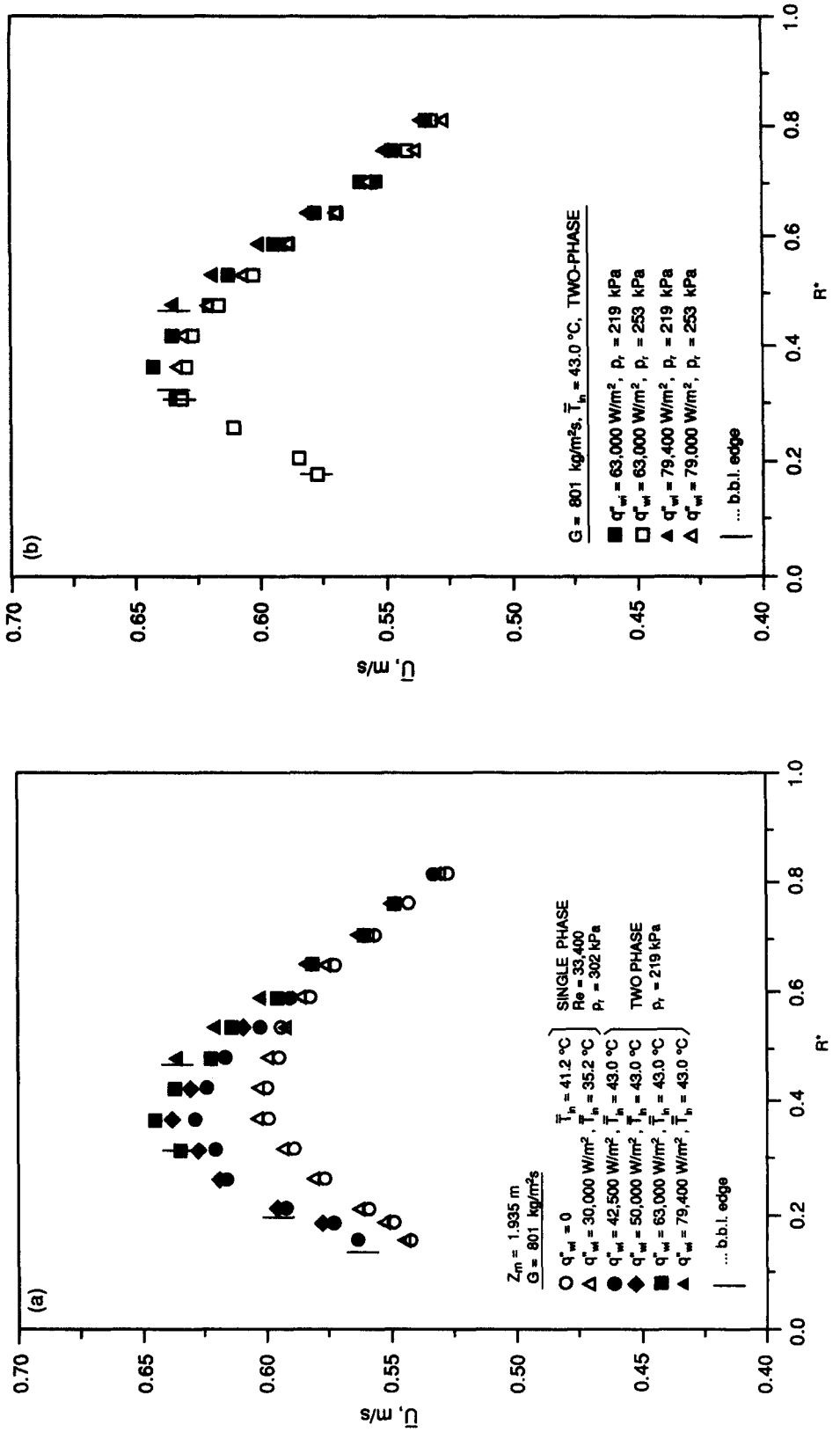

Figure 7(a, b)—*legend opposite.*

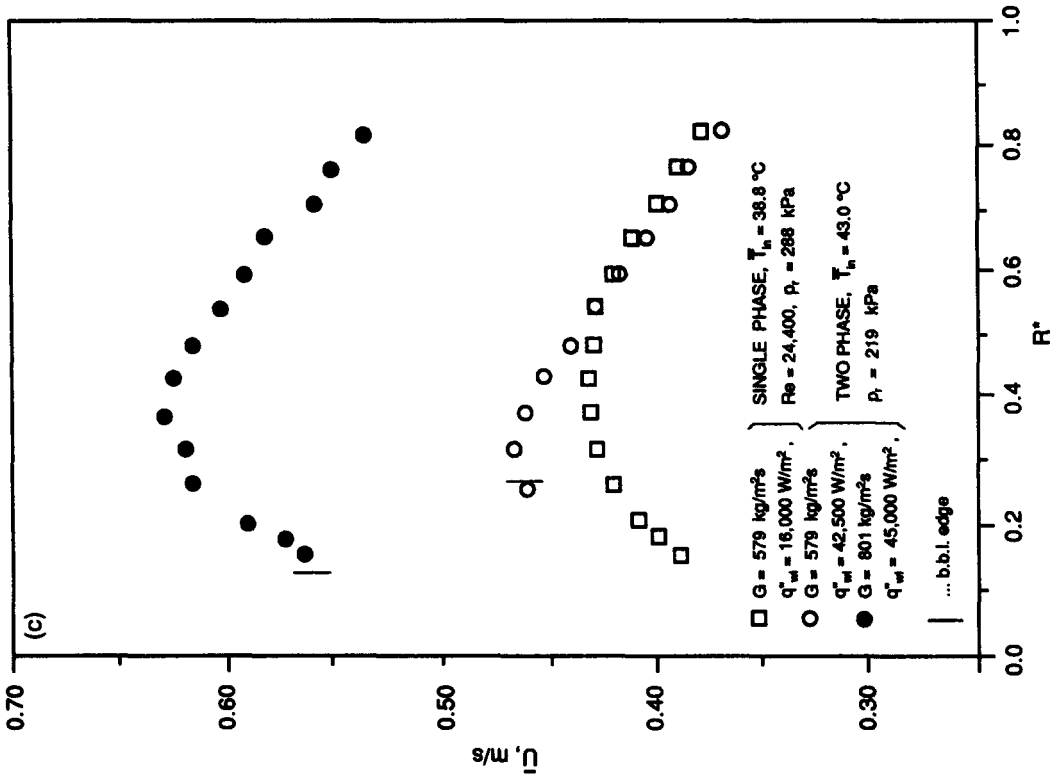

Figure 7(a–c). Mean axial velocity profiles in the all-liquid region.

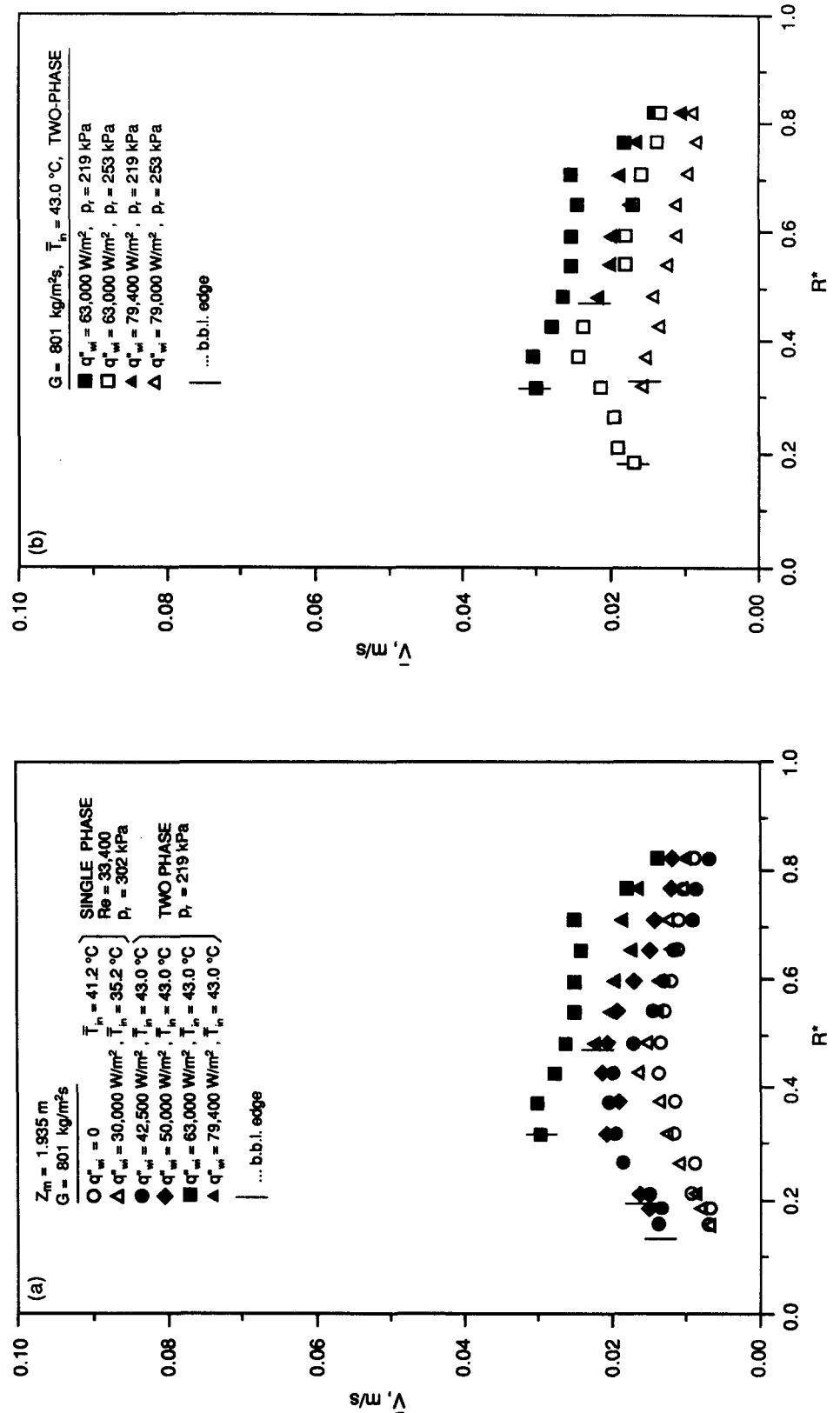

Figure 8(a, b)—*legend opposite.*

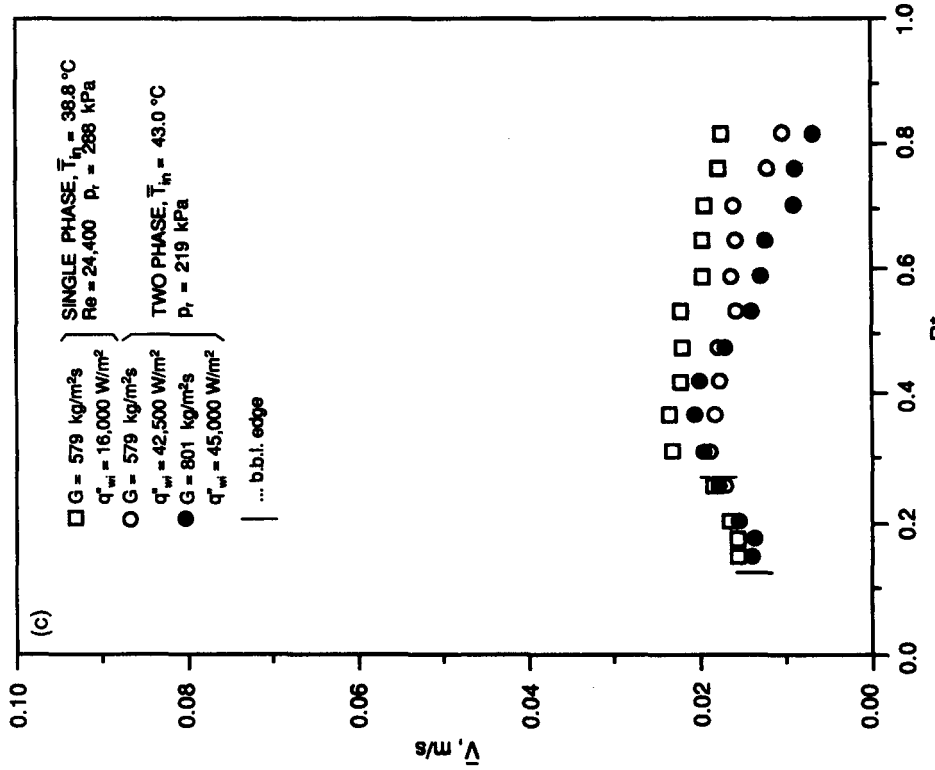

Figure 8(a–c). Mean radial velocity profiles in the all-liquid region.

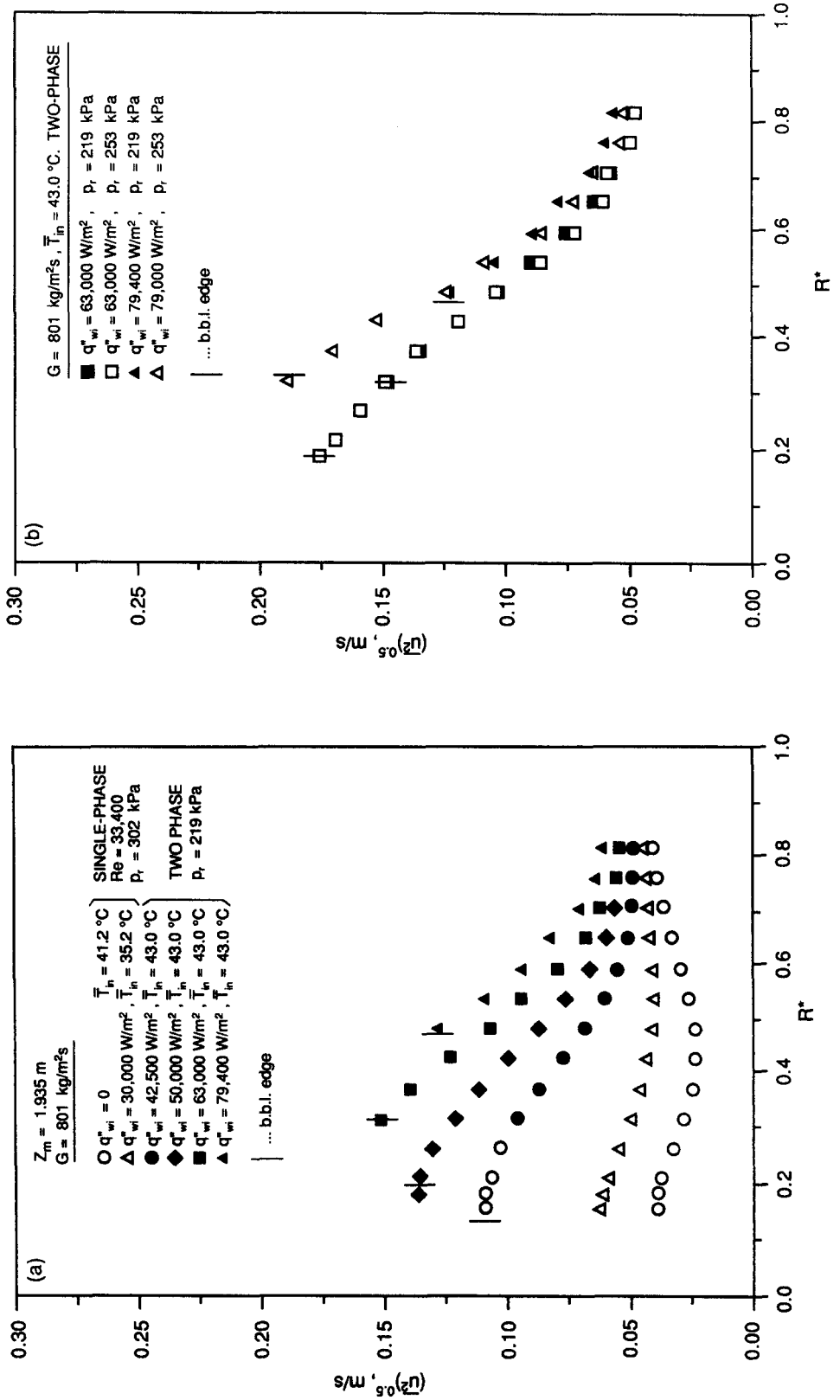

Figure 9(a, b)—*legend opposite.*

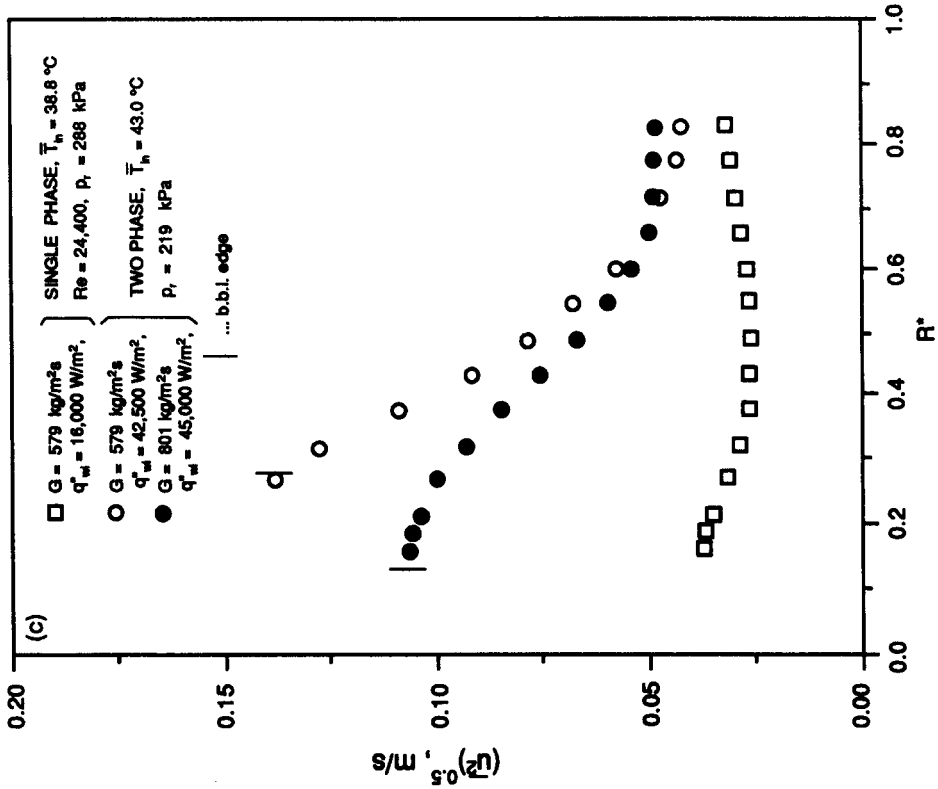

Figure 9(a–c). Axial velocity fluctuation intensity profiles in the all-liquid region.

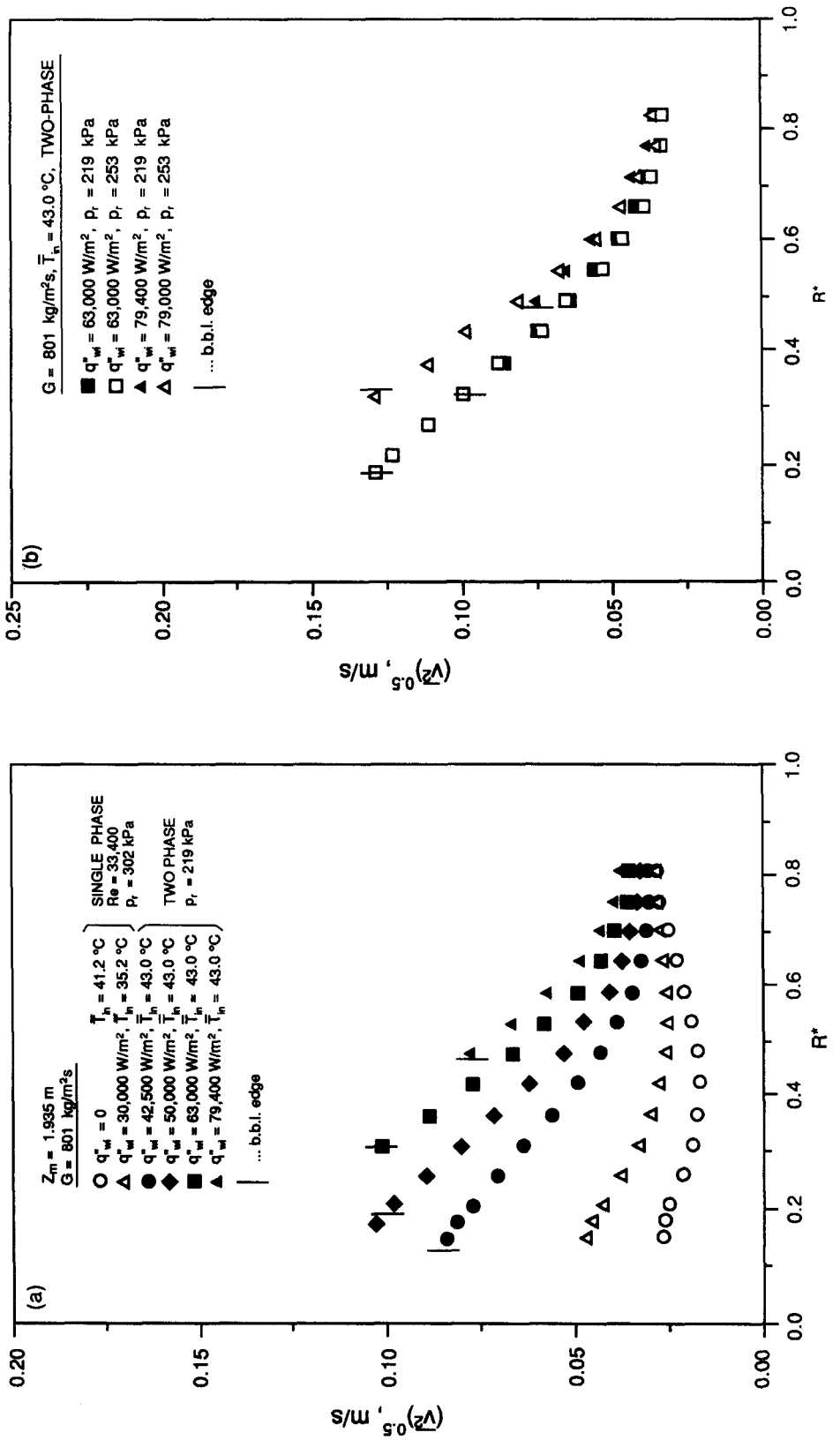

Figure 10(a, b)—*legend opposite.*

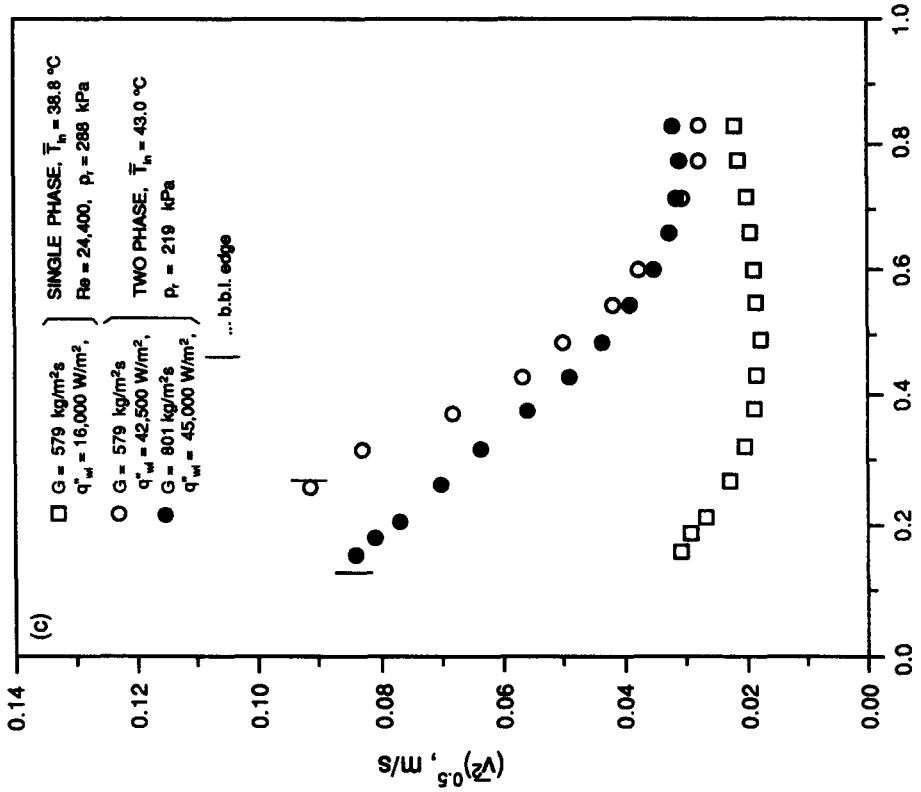

Figure 10(a–c). Radial velocity fluctuation intensity profiles in the all-liquid region.

value. In other words, the bubbles are essentially moving in the axial direction while oscillating back and forth radially. Our earlier visual observations of the movement of individual bubbles lend credence to this view (Hasan *et al.* 1991).

Figures 10(b) and 10(c) show the radial velocity fluctuation intensity profiles for the experimental conditions of figures 7(b) and 7(c), respectively. The influence of pressure on the intensity is again minimal, figure 10(b), while that of mass velocity is substantial, figure 10(c).

Turbulence microscales

Estimates of the Kolmogorov microscale η_L, the temperature (Batchelor) microscale η_θ and the dissipation rate of turbulent kinetic energy ϵ_L in the all-liquid region can be obtained from the turbulent intensity data presented. The Kolmogorov microscale, the smallest turbulence length scale which occurs in this region, may be expressed as (Tennekes & Lumley 1972):

$$\eta_L \equiv \left(\frac{\nu_L^3}{\epsilon_L}\right)^{1/4} \sim \left[\frac{\nu_L^3 l_L}{(\sqrt{\overline{u'^2}})^3}\right]^{1/4}, \qquad [1]$$

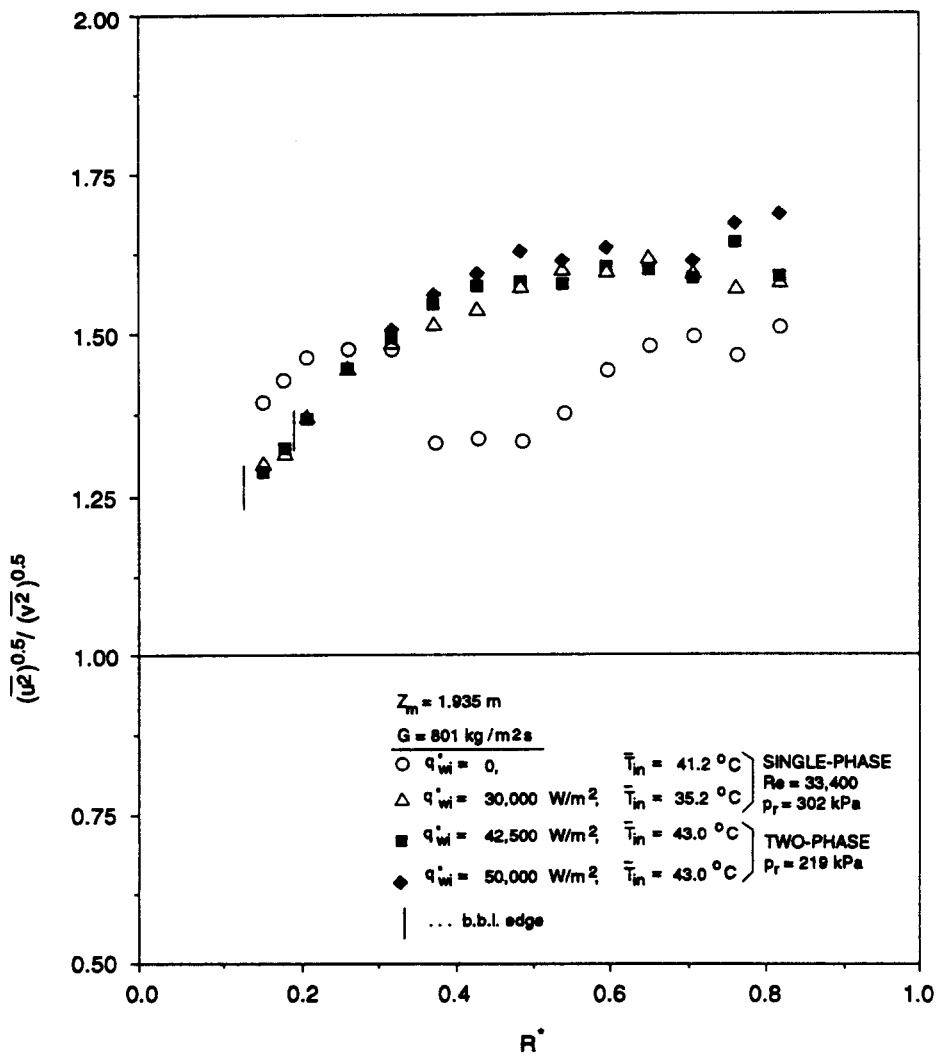

Figure 11. Anisotropy of the turbulent velocity field.

where l_L represents the largest length scale of turbulence (this may be estimated to be the width of the region) and v_L is the liquid kinematic viscosity. Calculations yield η_L values in the range of 0.03–0.1 mm. The temperature microscale, η_θ, would be smaller by a factor of $1/\sqrt{Pr}$, Pr being the liquid Prandtl number. For the present experiments, the Pr range is 6.5–7.5.

Reynolds shear stress

Figure 12(a) shows radial distributions of the Reynolds shear stress in the all-liquid region at the experimental conditions of figure 7(a). For unheated incompressible flow in an annulus, the Reynolds shear stress is negative in the region where the mean rate of strain is positive and positive where the mean rate of strain is negative (Brighton & Jones 1964; Hasan *et al.* 1992). This, of course, means that turbulent energy is produced at the expense of the mean flow kinetic energy. Also, for the unheated flow, the Reynolds shear stress passes through the zero value at a location very close to where the mean axial velocity is a maximum ($R^* \approx 0.40$). The two discernible effects of imposing a heat flux at the inner wall on the turbulent shear stress distribution in single-phase liquid flow are (Hasan *et al.* 1992): (i) a shift of the zero shear stress location closer to the inner wall (e.g. from $R^* \approx 0.40$ to 0.29 at a wall heat flux of 30,000 W/m^2), although the location of the maximum axial velocity remains essentially the same; and (ii) a concomitant decrease in the shear stress magnitude in the region between the zero crossing point and the inner wall and an increase in the region between the zero crossing point and the outer wall.

Significant changes occur in the all-liquid region shear stress distribution upon commencement of boiling at the inner wall. Let us consider the case of wall heat flux equal to 42,500 W/m^2. Here, the boiling layer extends to $R^* \approx 0.13$. We recall, figure 7(a), that the mean liquid axial velocity in part of the all-liquid region, from $R^* \approx 0.13$ to 0.5, is significantly higher compared to the nonboiling conditions (e.g. $q_{wi}'' = 30{,}000$ W/m^2). The maximum mean axial velocity location has moved a little closer to the inner wall ($R^* \approx 0.38$), as has the zero shear stress location ($R^* \approx 0.24$). The magnitude of the Reynolds shear stress is, in general, markedly larger compared to the nonboiling flow cases. Another interesting feature is that while the mean strain rate is positive in the region $0.24 < R^* \lesssim 0.38$, the Reynolds shear stress is also positive. With due caution, in view of the measurement uncertainties involved, we suggest that the turbulence production rate, $-\rho\overline{uv}S_{zr}$, is negative in this region, S_{zr} being the mean strain rate. The implication is that mean flow kinetic energy is being retrieved from the turbulence energy in this part of the all-liquid region. This is an entirely possible scenario in variable-density flows such as the one under scrutiny and leads to an increase in the local mean axial velocity. In the remainder of the all-liquid region however, turbulent energy is produced at the expense of the mean flow kinetic energy.

At a wall heat flux of 50,000 W/m^2, the boiling layer extends to $R^* \approx 0.19$. Again, it appears that in part of the all-liquid region ($0.24 < R^* < 0.38$) the turbulence production rate is negative, while in the remainder of the region it is positive. The Reynolds shear stress magnitude is generally larger than in the 42,500 W/m^2 case.

At wall heat fluxes of 63,000 and 79,400 W/m^2, the all-liquid region is thinner. The mean strain rate is negative in most of this region at 63,000 W/m^2 and in all of the region at 79,400 W/m^2. The turbulent shear stress is positive throughout the region. Energy is therefore transferred from the mean flow to turbulence. While the shear stress undergoes a significant enhancement when the wall heat flux is increased from 50,000 to 63,000 W/m^2, the increase is small when the heat flux is increased from 63,000 to 79,400 W/m^2.

Figures 12(b) and 12(c) depict the Reynolds shear stress radial distributions in the all-liquid region at the experimental conditions of figures 7(b) and 7(c), respectively. The effect of pressure on the magnitude of the shear stress is small but discernible, the shear stress being slightly larger at lower pressure. A change in mass velocity has a much stronger effect on the shear stress, this being similar to the effect on the axial and radial velocity fluctuation intensities individually.

On the basis of the turbulent normal and shear stress data, we conclude that the turbulent shear stress in the all-liquid region is affected as significantly as the turbulent normal stresses. The region being in turbulent shear flow, this is an entirely reasonable finding. An in-depth explanation of the

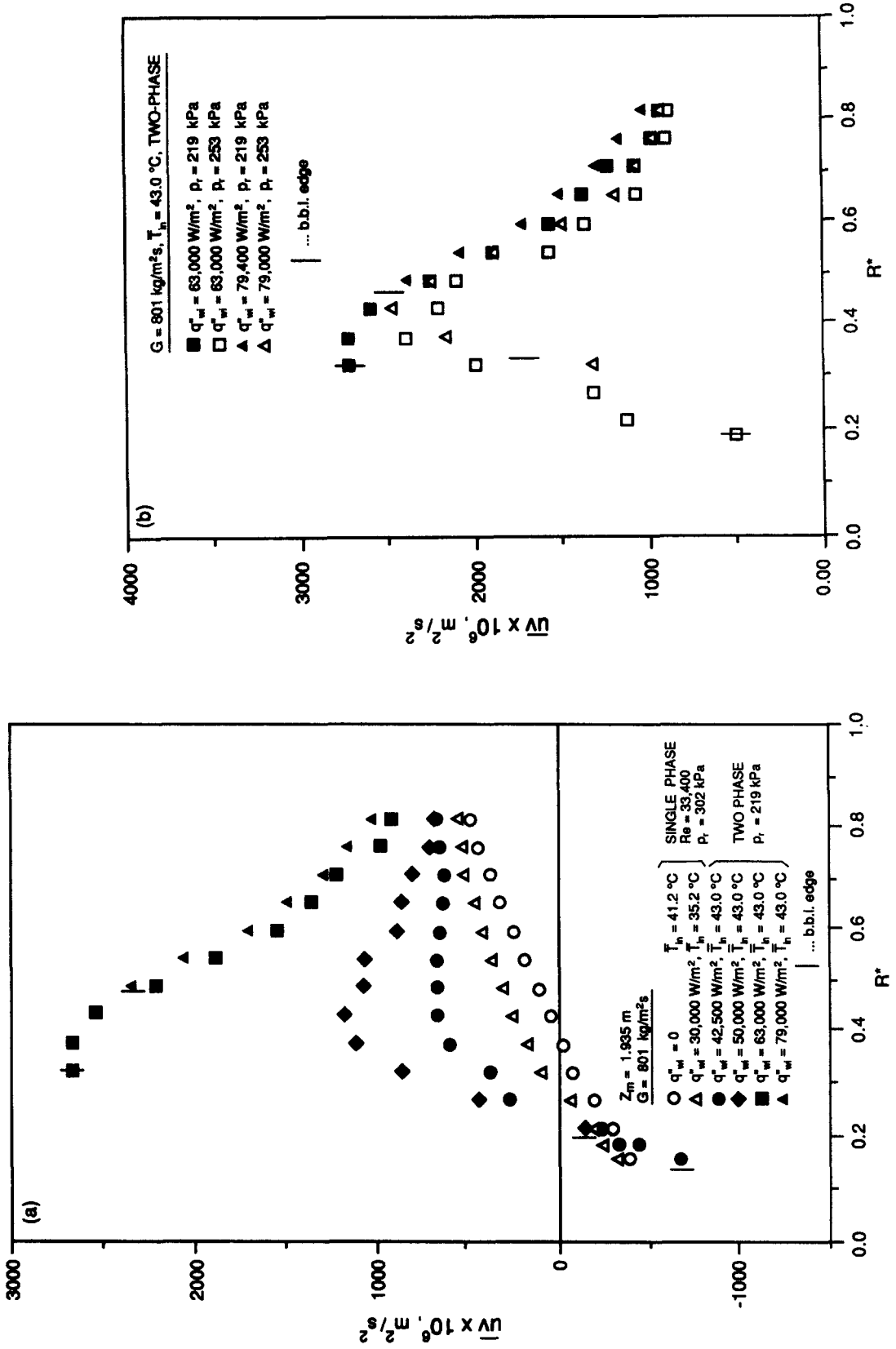

Figure 12(a, b)—*legend opposite.*

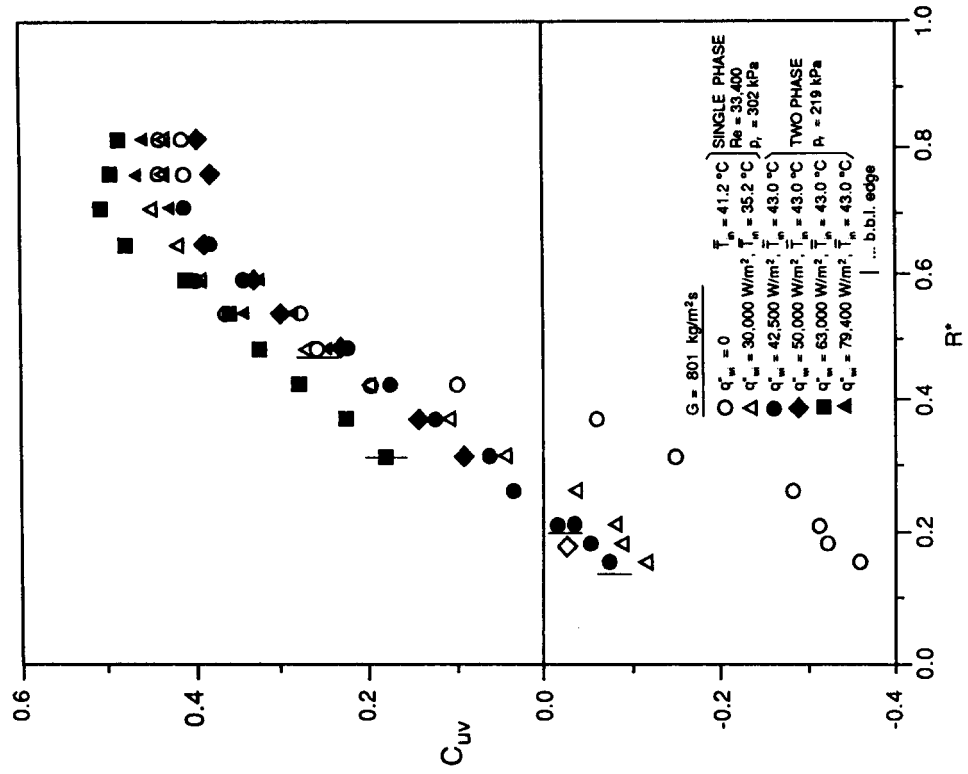

Figure 13. Correlation coefficient (C_{uv}) profiles in the all-liquid region.

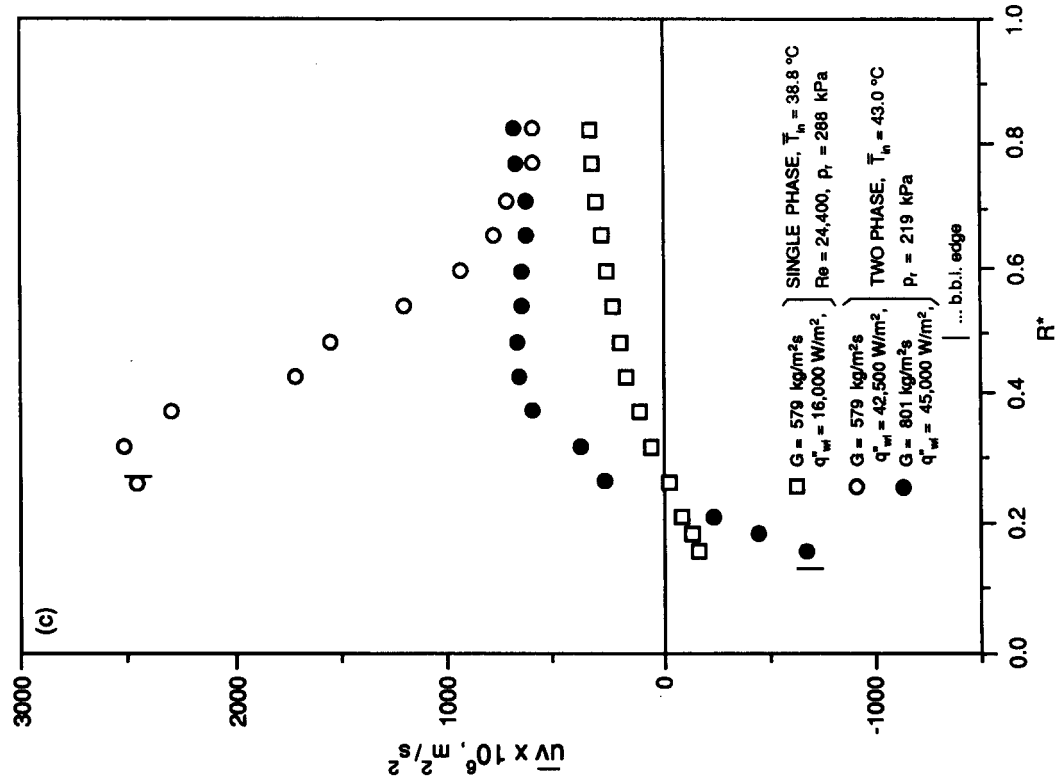

Figure 12(a–c). Reynolds shear stress profiles in the all-liquid region.

increase in turbulent shear stress is complicated however, because the dynamics of turbulence (e.g. transport and stretching of vorticity) need to be considered.

The coefficient C_{uv}, defined as

$$\frac{\overline{uv}}{(\overline{u^2})^{0.5}(\overline{v^2})^{0.5}}, \qquad [2]$$

lies between -1 and $+1$ by virtue of its definition, its magnitude being a measure of the degree of correlation (interdependence) between u and v. In figure 13, the correlation coefficient values calculated from the data of figures 9(a), 10(a) and 12(a) are shown. In an earlier paper (Hasan *et al.* 1992) we indicated that $|C_{uv}|$ was in the range 0–0.5 for all of our nonboiling turbulent flow data and that it decreased in the heated wall proximity with an increase in wall heat flux. For the boiling flow experiments, the magnitude of the correlation coefficient in the all-liquid region appears to be in the same range. Typically, it has a low value (<0.3) at the boiling layer edge.

Turbulent radial heat flux

Figure 14(a) presents radial distributions of the single-point cross-correlation between the radial velocity fluctuation and the temperature fluctuation (=turbulent radial heat flux/ρc_p) in the all-liquid region for the experimental conditions of figure 7(a). In an earlier paper (Hasan *et al.* 1992), we reported our lack of success in accurately measuring the $\overline{vt}$ correlation in the region $R^* < 0.4$ of single-phase turbulent liquid flow. The measured values were generally significantly smaller than those expected on the basis of thermal energy balance calculations. Some possible reasons for this, such as the relatively large measurement volume of the three-sensor anemometer probe in comparison to the smaller spatial scales of turbulence, were suggested. The data in figure 14(a) suffers from the same drawback. What is noteworthy, however, is the substantial increase in the magnitude of $\overline{vt}$ in the all-liquid region upon commencement of boiling and the continual increase in the magnitude of this correlation in response to heightened activity in the boiling layer caused by an increase in the wall heat flux. This increase in $\overline{vt}$ is consistent with the increases observed in $\sqrt{v^2}$ and $\sqrt{t^2}$ in response to augmented boiling in the adjoining layer caused by wall heat flux increase, figures 10(a) and 6(a), provided that the correlation (interdependence or coherence) between these two fluctuations is sustained.

Figures 14(b) and 14(c) show radial distributions of the $\overline{vt}$ correlation in the all-liquid region at the experimental conditions of figures 7(b) and 7(c). A small increase in the correlation magnitude (and therefore, in the radial turbulent heat flux) is observed at the lower pressure. We note that no increase in either $\sqrt{v^2}$ or $\sqrt{t^2}$ was observed under similar circumstances, figures 10(b) and 6(b). A possible explanation is that the extent of interdependence (or coherence) between these two fluctuations increases when augmented boiling takes place in the adjoining layer and a larger number of closely spaced bubbles appear. It is interesting that a similar small increase in the $\overline{uv}$ correlation was observed at lower pressure, figure 12(b). A much more significant increase in the $\overline{vt}$ correlation is seen when the mass velocity decreases, figure 14(c). This is consistent with the substantial increases in $\sqrt{v^2}$ and $\sqrt{t^2}$ in the all-liquid region under similar circumstances, figures 10(c) and 6(c). We also note a commensurate increase in the $\overline{uv}$ correlation upon a decrease of mass velocity, figure 12(c).

4. CONCLUDING REMARKS

The turbulence measurements reported in this paper are in the all-liquid region of subcooled boiling flow, the one exception being the fluid temperature field data which span a portion of the boiling layer. Of particular importance are the liquid measurements near the boundary between the bubbly boiling layer and the all-liquid region, since the influence of the boiling layer is rather strong here. The data indicate that the turbulent velocity and temperature field (including the Reynolds stresses and turbulent heat flux) are altered significantly near the inter-region boundary.

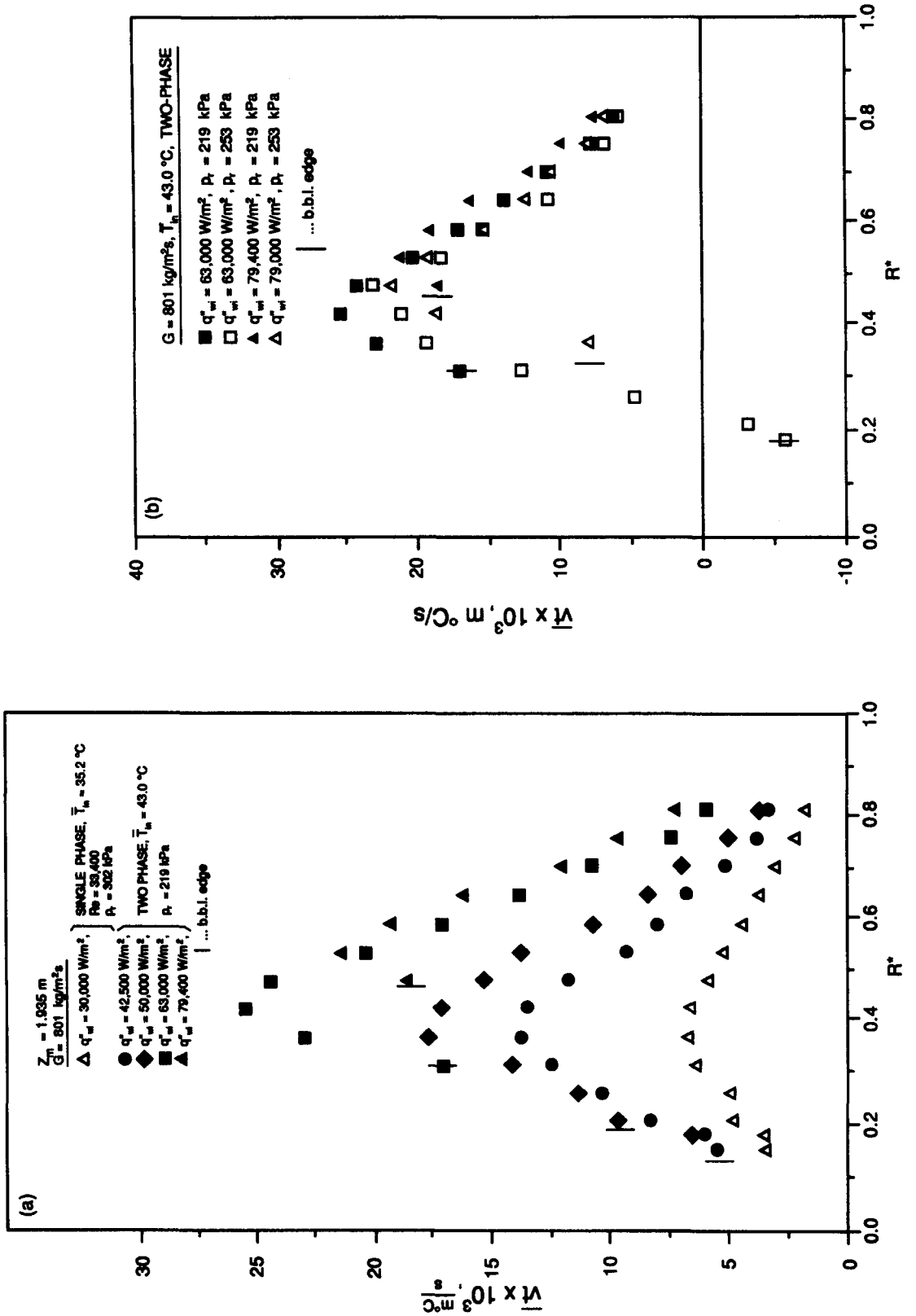

Figure 14(a, b)—*legend overleaf.*

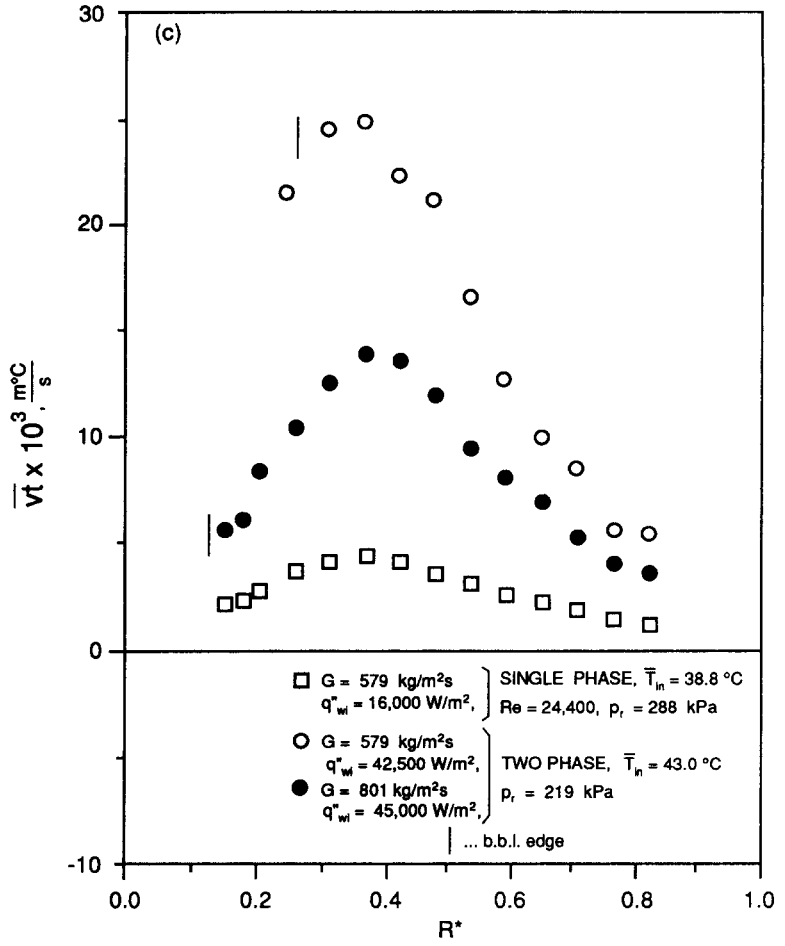

Figure 14(a–c). Radial velocity–temperature correlation profiles in the all-liquid region.

Measures of the turbulent shear stress and radial turbulent heat flux at the inter-region boundary can be obtained from the reported data. These are presently being utilized in our development of a two-region quasi-one-dimensional model of subcooled boiling flow through annular channels. In this model, the governing two-fluid equations for each region are obtained by rigorous area-averaging of the time-averaged local mass, momentum and thermal energy equations over the region. Coupling of the region-averaged equations at the inter-region boundary requires information on, among other quantities, turbulent shear stress and heat flux.

Data on the turbulent structure of the all-liquid region are also valuable in the development and subsequent validation of a multidimensional model of subcooled boiling flow. The decidedly anisotropic nature of the turbulence measured indicates that a Reynolds stress closure of wall turbulence for the liquid phase would be much more appropriate than, for instance, a k–ϵ closure. Marked increases in velocity fluctuations in the all-liquid region, especially near the inter-region boundary, lead one to anticipate similar increases within the boiling layer. Such an effect is consistent with the well-known increase in skin friction at the wall adjoining the boiling layer.

An appropriate model for the bubble-induced pseudo-turbulence must, of course, be developed for the liquid phase within the boiling layer. Comprehensive turbulence measurements in this layer must, therefore, be the next step. One of the authors (R.P.R.) is presently in the initial stage of these measurements in the same test section. A two-component laser-Doppler velocimeter, a fast-response microthermocouple and a dual-sensor fiber-optic probe are being employed.

Acknowledgements—This research was partially funded by National Science Foundation, Thermal Systems Program, Division of Chemical and Thermal Systems under Grant No. CTS-8918830. Support from the Electric Power Research Institute, Nuclear Power Division, is also gratefully acknowledged.

REFERENCES

BECKMAN, P., ROY, R. P., WHITFIELD, K. & HASAN, A. 1993 A fast-response microthermocouple. *Rev. Scien. Instrum.* In press.

BRIGHTON, J. A. & JONES, J. B. 1964 Fully developed turbulent flow in annuli. *J. Bas. Engng.* **86,** 835–844.

HASAN, A. 1991 Study of turbulent subcooled boiling and nonboiling flow through a vertical concentric annular channel. Ph.D. Dissertation, Arizona State Univ., Tempe, AZ.

HASAN, A., ROY, R. P. & KALRA, S. P. 1990 Heat transfer measurements in turbulent liquid flow through a vertical annular channel. *ASME Jl Heat Transfer* **112,** 247–250.

HASAN, A., ROY R. P. & KALRA, S. P. 1991 Some measurements in subcooled boiling flow of refrigerant-113. *ASME Jl Heat Transfer* **113,** 216–223.

HASAN, A., ROY, R. P. & KALRA, S. P. 1992 Velocity and temperature fields in turbulent liquid flow through a vertical concentric annular channel. *Int. J. Heat Mass Transfer* **35,** 1455–1467.

HERRINGE, R. A. & DAVIS, M. R. 1976 Structural development of gas–liquid mixture flows. *J. Fluid Mech.* **73,** 97–123.

JAIN, P. K. & ROY, R. P. 1983 Stochastic characteristics of vapor fraction and wall pressure fluctuations in boiling flow. *Int. J. Multiphase Flow* **9,** 463–489.

LANCE, M. & BATAILLE, J. 1991 Turbulence in the liquid phase of a uniform bubbly air–water flow. *J. Fluid Mech.* **222,** 95–118.

LAUNDER, B. E., REECE, G. J. & RODI, W. 1975 Progress in the development of a Reynolds-stress turbulence closure. *J. Fluid Mech.* **68,** 537–566.

LOPEZ DE BERTODANO, M., LEE, S-J, LAHEY, R. T. JR & DREW, D. A. 1990 The prediction of two-phase turbulence and phase distribution phenomena using a Reynolds stress model. *J. Fluids Engng.* **112,** 107–113.

MARIÉ, J. L. 1983 Investigation of two-phase bubbly flows using laser-Doppler anemometry. *PhysicoChem Hydrodynam.* **4,** 103–118.

MARIÉ, J. L. 1987 Modelling of the skin friction and heat transfer in turbulent two-component bubbly flow in pipes. *Int. J. Multiphase Flow* **13,** 309–325.

MICHIYOSHI, I. 1978 Heat transfer in air–water two-phase flow in a concentric annulus. *Proc. 6th Int. Heat Transfer Conf.*, Toronto, Vol. 1, pp. 499–504.

MICHIYOSHI, I. & SERIZAWA, A. 1986 Turbulence in two-phase flow. *Nucl. Engng. Des.* **95,** 253–267.

ROY, R. P., KRISHNAN, V. & RAMAN, A. 1986 Measurements in turbulent liquid flow through a vertical concentric annular channel. *ASME Jl Heat Transfer* **108,** 216–218.

SATO, Y., SADATOMI, M. & SEKOGUCHI, K. 1981a Momentum and heat transfer in two-phase bubble flow—I. Theory. *Int. J. Multiphase Flow* **7,** 167–177.

SATO, Y., SADATOMI, M. & SEKOGUCHI, K. 1981b Momentum and heat transfer in two-phase bubble flow—II. A comparison between experimental data and theoretical calculations. *Int. J. Multiphase Flow*, **7,** 179–190.

SERIZAWA, A. & KATAOKA, I. 1990 Turbulence suppression in bubbly two-phase flow. *Nucl. Engng. Des* **122,** 1–16.

SERIZAWA, A., KATAOKA, I. & MICHIYOSHI, I. 1975a Turbulence structure of air–water bubbly flow—I: measuring techniques. *Int. J. Multiphase Flow* **2,** 221–233.

SERIZAWA, A., KATAOKA, I. & MICHIYOSHI, I. 1975b Turbulence structure of air–water bubbly flow—II: local properties. *Int. J. Multiphase Flow* **2,** 235–246.

SERIZAWA, A., KATAOKA, I. & MICHIYOSHI, I. 1975c Turbulence structure of air–water bubbly flow—III: transport properties. *Int. J. Multiphase Flow* **2,** 247–259.

TENNEKES, H. & LUMLEY, J. L. 1972 *A First Course in Turbulence.* MIT Press, Boston, MA.

THEOFANOUS, T. G. & SULLIVAN, J. 1982 Turbulence in two-phase flows. *J. Fluid Mech.* **116,** 343–362.

WANG, K. S., LEE, S. J., JONES, O. C. JR & LAHEY, R. T. JR 1987 3-D turbulence structure and phase distribution measurements in bubbly two-phase flow. *Int. J. Multiphase Flow* **13,** 327–343.